UNIVERSITAT POLITÈCNICA DE VALÈNCIA

Estudio y caracterización experimental de nuevas estructuras difractivas

Memoria presentada por:
Federico José Machado Olivares

Directores:
Juan Antonio Monsoriu Serra
Walter Daniel Furlan

Julio, 2018

Dr. Juan Antonio Monsoriu Serra, Catedrático de Universidad del Departamento de Física Aplicada de la Universitat Politècnica de València y Dr. Walter Daniel Furlan, Catedrático de Universidad del Departamento de Óptica de la Universitat de València.

CERTIFICAN que la presente memoria ”Estudio y caracterización experimental de nuevas estructuras difractivas” resume el trabajo de investigación realizado, bajo su dirección, por D. Federico José Machado Olivares y constituye su Tesis para optar al título de Doctor.

Y para que conste, en cumplimiento de la legislación vigente, firman el presente certificado en Valencia a 26 de Julio de 2018.

Fdo.: Dr. Juan A. Monsoriu Serra Fdo.: Dr. Walter D. Furlan

Agradecimientos

Agradezco a mis tutores, Juan A. Monsoriu y Walter D. Furlan por su gran apoyo, orientación y dirección durante todo el proceso de mi Tesis.

A mi compañero de laboratorio Vicente Ferrando, gracias por sus consejos y compañía en mis años de estancia durante el desarrollo de mi trabajo de Tesis en estas tierras extranjeras.

A Toni, Lilian, Juan y Daysi por su compañía en los momentos de dar ánimo para seguir adelante.

A todas las personas que trabajan para crear y desarrollar herramientas de software libre, el cual he utilizado para realizar simulaciones y postprocesado de imágenes en el desarrollo de esta Tesis.

Al programa MayaNet Erasmus Mundus por la financiación concedida para la realización de mi estancia de doctorado en España durante 3 años.

A mi familia y amigos que me han acompañado en la distancia.

Gracias !!!

Resumen

Los Elementos Ópticos Difractivos han experimentado un creciente interés en los últimos años debido a sus múltiples aplicaciones en los campos de la microscopía y de las telecomunicaciones, entre otros. Actualmente, también se están desarrollando importantes progresos en el diseño de lentes intraoculares y lentes de contacto basadas en estructuras difractivas.

Durante el proceso de realización de esta Tesis Doctoral se ha estudiado en primer lugar el estado del arte relacionado con estos elementos ópticos, prestando especial interés en el diseño y caracterización de lentes difractivas. En su forma más sencilla, estas lentes están formadas por un conjunto de anillos transparentes y opacos distribuidos periódicamente a lo largo de la variable radial cuadrática. Reemplazando esta distribución periódica de anillos por una secuencia aperiódica determinista, se ha conseguido mejorar las prestaciones de las lentes difractivas. Así, por ejemplo, con la secuencia fractal de Cantor se puede obtener una extensión de la profundidad de foco y una reducción de la aberración cromática. Por otro lado, con la secuencia de Fibonacci, se pueden diseñar lentes difractivas bifocales. Combinando estas lentes basadas en geometrías aperiódicas con máscaras de fase helicoidales se han generado nuevas distribuciones de vórtices ópticos susceptibles de ser utilizados como trampas ópticas para atrapar y manipular partículas micrométricas.

Tomando todas estas estructuras difractivas como punto de partida en el desarrollo de esta Tesis Doctoral, se ha avanzado en el estudio y caracterización experimental de lentes difractivas basadas en secuencias aperiódicas diferentes a las consideradas previamente. En concreto, se han obtenido nuevas propiedades de focalización y formación de imágenes utilizando las funciones de Walsh y la secuencia *m*-bonacci.

También se ha abordado el estudio y caracterización experimental de lentes difractivas en el rango de los THz. Se han desarrollado diferentes prototipos mediante impresión 3D que están permitiendo tanto la focalización, como la generación de vórtices de THz.

Resum

Els Elements Òptics Difractius han experimentat un creixent interès en els últims anys a causa de les seves múltiples aplicacions en els camps de la microscòpia i de les telecomunicacions, entre altres. Actualment, també s'estan desenvolupant importants progressos en el disseny de lents intraoculars i lents de contacte basades en estructures difractives.

Durant el procés de realització d'aquesta Tesi Doctoral s'ha estudiat en primer lloc l'estat de l'art relacionat amb aquests elements òptics, prestant especial interès en el disseny i caracterització de lents difractives. En la seva forma més senzilla, aquestes lents estan formades per un conjunt d'anells transparents i opacs distribuïts periòdicament al llarg de la variable radial quadràtica. Reemplaçant aquesta distribució periòdica d'anells per una seqüència aperiòdica determinista, s'ha aconseguit millorar les prestacions de les lents difractives. Així, per exemple, amb la seqüència fractal de Cantor es pot obtenir una extensió de la profunditat de focus i una reducció de l'aberració cromàtica. D'altra banda, amb la seqüència de Fibonacci, es poden dissenyar lents difractives bifocals. Combinant aquestes lents basades en geometries aperiòdiques amb màscares de fase helicoïdals s'han generat noves distribucions de vòrtex òptics susceptibles de ser utilitzats com trampes òptiques per atrapar i manipular partícules micromètriques.

Prenent totes aquestes estructures difractives com a punt de partida en el desenvolupament d'aquesta tesi doctoral, s'ha avançat en l'estudi i caracterització experimental de lents difractives basades en seqüències aperiòdiques diferents a les considerades prèviament. En concret, s'han obtingut noves propietats de focalització i formació d'imatges utilitzant les funcions de Walsh i la seqüència *m*-*b*onacci.

També s'ha abordat l'estudi i caracterització experimental de lents difractives en el rang dels THz. S'han desenvolupat diferents prototips mitjançant impressió 3D que estan permetent tant la focalització, com la generació de vòrtex de THz.

Abstract

The Diffractive Optical Elements have experienced a growing interest in recent years due to its multiple applications in the fields of microscopy and telecommunications, among others. Currently, important progress is also being made in the design of intraocular lenses and contact lenses based on diffractive structures.

During the process of conducting this Doctoral Thesis, the state of the art related to these optical elements was first studied, paying special attention to the design and characterization of diffractive lenses. In its simplest form, these lenses are formed by a set of transparent and opaque rings distributed periodically along the quadratic radial variable. By replacing this periodic distribution of rings with a deterministic aperiodic sequence, the performance of diffractive lenses has been improved. Thus, for example, with the Cantor fractal sequence an extension of the depth of focus and a reduction of the chromatic aberration can be obtained. On the other hand, with the Fibonacci sequence, bifocal diffractive lenses can be designed. Combining these lenses based on aperiodic geometries with helical phase masks, new distributions of optical vortices have been generated that can be used as optical traps to trap and manipulate micrometric particles.

Taking all these diffractive structures as a starting point in the development of this Doctoral Thesis, progress has been made in the study and experimental characterization of diffractive lenses based on aperiodic sequences different from those previously considered. In particular, new focusing and imaging properties have been obtained using the Walsh functions and the *m*-bonacci sequence.

The study and experimental characterization of diffractive lenses in the THz range has also been addressed. Different prototypes have been developed by means of 3D printing that are allowing both the focusing and the generation of THz vortices.

Indice general

Capítulo I

Introducción general

En este capítulo se describe, en primer lugar, el estado del arte relacionado con los elementos ópticos difractivos aperiódicos que constituyen el punto de partida para el desarrollo de esta Tesis Doctoral. A continuación, se describen los objetivos concretos de la Tesis, enfocados principalmente a la implementación de diferentes secuencias aperiódicas al diseño de nuevas lentes difractivas y a la construcción de prototipos de lentes difractivas para el rango de los THz. Por último, se expone la estructura de la Tesis presentada en formato de compendio de publicaciones.

1.1 Antecedentes y objetivos de la investigación

Los Elementos Ópticos Difractivos (EDOs) han experimentado en los últimos años un creciente interés, ya que son componentes esenciales en el diseño de sistemas formadores de imágenes, no solo en el rango visible, sino también en aplicaciones que van desde la óptica de THz [Siemion12] a la microscopía de rayos X [Sakdinawat07].

Dentro del conjunto de los EODs, las Placas Zonales (PZs) son estructuras formadas por zonas anulares concéntricas de igual área, que alternadamente son transparentes y opacas. Consecuentemente, el radio de estas zonas es proporcional a la raíz cuadrada de números naturales. Por tanto, es posible expresar la

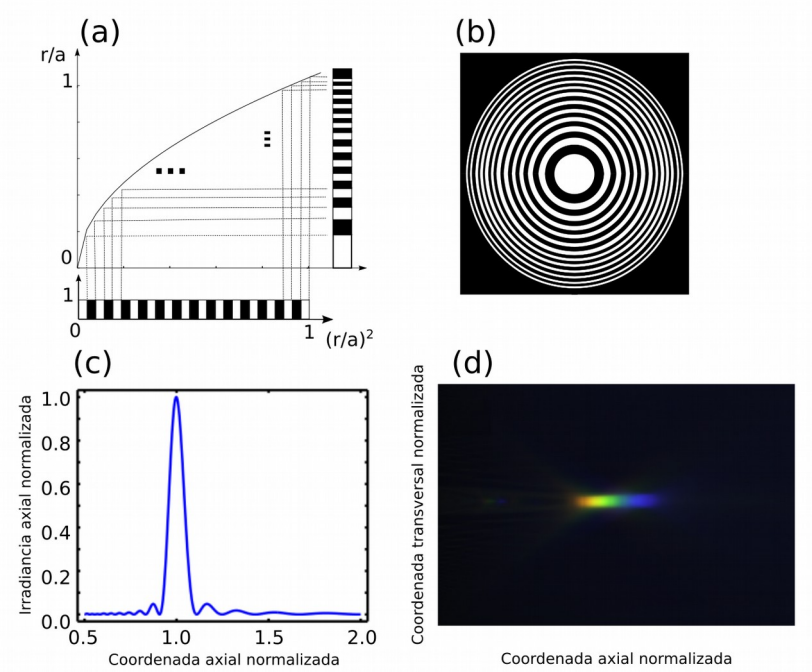

Fig. 1.1: Diseño y caracterización experimental de una PZ convencional: (a) Función de transmitancia radial basada en una secuencia periódica, (b) Transmitancia bidimensional en la pupila de la PZ, (c) Irradiancia axial normalizada bajo iluminación monocromática y (d) Patrón de irradiancia bajo iluminación policromática en el que se observa una fuerte aberración cromática.

transmitancia de estas lentes como una función periódica, $p(r^2)$, donde r es la variable radial (ver Fig. 1.1a y 1.1b). Si se ilumina una PZ de radio a con una onda plana monocromática de longitud de onda λ, se producen por difracción una serie de focos a lo largo del eje óptico, ubicados a distancias del plano de la lente $f_n = a^2/n\lambda N$, donde $n \in \mathbb{Z}$ y N es el número de zonas de la lente. En la Fig. 1.1c se muestra la irradiancia axial normalizada para el foco principal correspondiente al orden $n = 1$. Las placas zonales presentan, de forma inherente, una fuerte aberración cromática

ocasionada por la dependencia explícita entre la distancia focal, f_n, y la longitud de onda de la radiación incidente, λ (ver Fig. 1.1d).

Para intentar reducir esta aberración cromática y otras limitaciones de las PZs, como es una escasa profundidad de foco, se han considerado diversas secuencias aperiódicas deterministas en la distribución radial de zonas de la lente, lo que permite generar nuevos perfiles de focalización. Por ello, conviene previamente repasar los conceptos de orden periódico y aperiódico que aparecieron originalmente en el ámbito de la cristalografía [Maciá06].

Los átomos contenidos en estructuras cristalinas presentan simetría de traslación 3D, es decir, se encuentran ordenados periódicamente. Según el teorema de restricción cristalográfica [Bamberg03], la simetría de rotación alrededor de cualquier átomo en la red sólo puede ser de orden 2, 3, 4 o 6. Al iluminar los cristales con un haz de rayos X se genera un patrón de difracción periódico y discreto que depende de los parámetros geométricos de su distribución atómica, preservando siempre la simetría de rotación del cristal. Por otra parte, en el extremo opuesto, los materiales amorfos están caracterizados por una distribución totalmente aleatoria de sus átomos. En este caso, si se iluminara con un haz de rayos X este tipo de material, se obtiene una distribución continua en su patrón de difracción.

Entre los casos mencionados anteriormente, entre el perfecto orden y el desorden, se encuentran los denominados cuasicristales, cuyos átomos no presentan simetría de traslación 3D de forma estricta, aunque presentan ciertas simetrías de rotación. Sin embargo, al iluminar estos materiales con rayos X, también se obtienen patrones de difracción discretos aparentemente prohibidos por el teorema de restricción cristalográfica. En concreto, en los años 80, Shechtman descubrió unas aleaciones de Aluminio y Manganeso con patrón de difracción discreto que

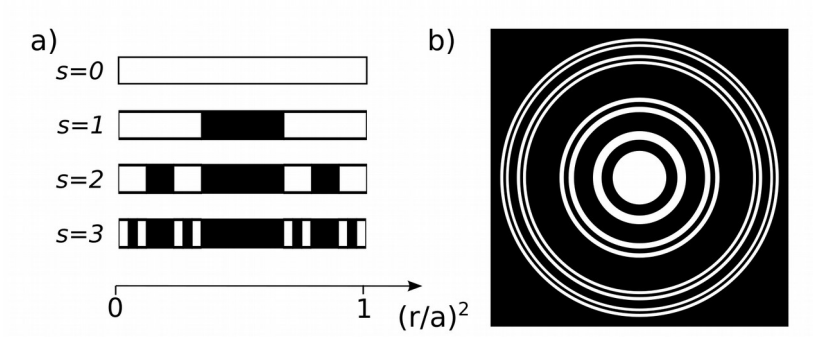

Fig. 1.2: a) Perfil radial cuadrático de una PZ fractal basada en el conjunto de Cantor. b) Transmitancia de una PZ fractal.

presenta simetrías de rotación de órdenes 5 y 10 [Shechtman84], dando lugar a lo que se conocen como estructuras cuasicristalinas.

Lentes fractales

Los Fractales constituyen otro tipo de sistemas aperiódicos de especial interés con patrón de difracción discreto. Su estructura interna se replica a diferentes escalas, propiedad conocida como auto-similitud. Matemáticamente, los fractales pueden construirse por sustitución iterativa a diversas escalas de una estructura inicial básica, por lo que su dimensión no es entera. Dada la irregularidad de las estructuras fractales, no es posible describirlas en términos geométricos convencionales, pero permiten modelizar estadísticamente líneas de costa, rayos y nubes, entre otros sistemas complejos.

Uno de los fractales más sencillos desde el punto de vista matemático es el conjunto triádico de Cantor. Partiendo de un segmento de longitud unidad, se divide en tres partes iguales y se elimina la central. Se repite el proceso de forma iterativa sobre

cada uno de los segmentos resultantes. La secuencia aperiódica resultante se muestra en la figura 1.2a.

Reemplazando la estructura periódica que define la transmitancia de una PZ convencional por el conjunto fractal de Cantor, se obtuvieron las primeras PZ fractales (PZFs) de la literatura [Saavedra03]. En la Fig. 1.2 se muestra el diseño de una PZF de orden $S = 3$. Puede comprobarse tanto teórica como experimentalmente [Davis04] que una PZF produce múltiples focos a lo largo del eje óptico z cuando se ilumina por una onda plana monocromática. La estructura interna de cada uno de estos focos presenta una estructura interna fractal, replicando así la auto-similitud de la lente original. Los parámetros de diseño de la lente PZF pueden ser ajustados para modificar el número de focos y su amplitud relativa [Monsoriu04, Remón13].

Además, como elemento formador de imágenes, la profundidad de foco puede aumentarse significativamente al cambiar los parámetros de diseño de la lente [Remón13, Furlan07, Ge12]. Adicionalmente, reemplazando la simetría de revolución de la PZF por una geometría rectangular, es posible obtener un volumen focal autosimilar en forma de aspa que potencialmente podría ser utilizado en sistemas de alineamiento óptico [Calatayud13b].

Criba de fotones

Una Criba de Fotones (ver Fig. 1.3) es una PZ en la que se reemplazan las zonas transparentes por múltiples agujeros disjuntos de diferentes diámetros. Esta nueva estructura de lente difractiva fue diseñada y desarrollada originalmente para focalizar y formar imágenes de alta resolución con rayos X [Kipp01].

Posteriormente, a partir del estudio detallado de sus características tanto desde el punto de vista teórico como

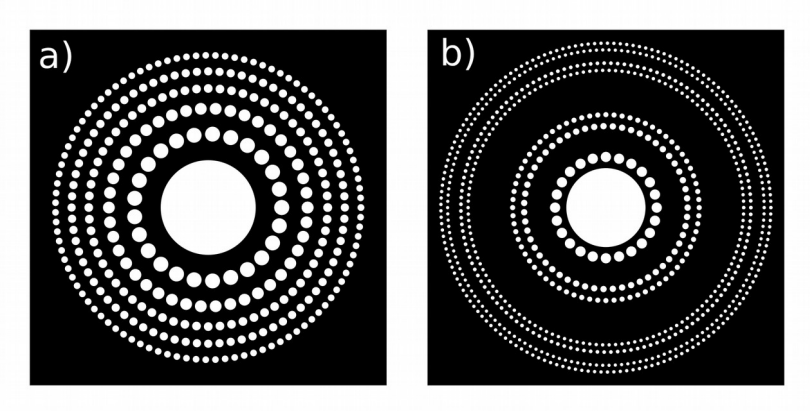

Fig. 1.3: a) CF convencional. b) CF fractal.

experimental [Cao03, Cao02], estas lentes han sido implementadas en diversas aplicaciones tecnológicas [Menon05, Andersen05].

En este contexto, se ha propuesto también la Criba de Fotones Fractal (CFF) [Giménez06] que, comparada con la PZF, mostraba una notable eficiencia en difracción apodizando los focos de orden superior.

Utilizando el fractal conocido como Polvo de Cantor, también se han diseñado CFF con geometrías rectangulares [Ferrando13].

Lentes de Fibonacci

En la naturaleza existen múltiples sistemas que se pueden describir con un modelo matemático basado en la sucesión de números de Fibonacci. Para generar esta sucesión de números, partimos de las semillas $F_0=0$ y $F_1=1$. El *i*-ésimo número de Fibonacci viene dado por la suma de los dos anteriores, es decir, $F_i=F_{i-1}+F_{i-2}$, con $i>1$, por lo que $F_i=\{0,1,1,2,3,5,8,13,..\}$. La relación entre dos números consecutivos de esta sucesión tiende asintóticamente a lo que se conoce como proporción áurea o

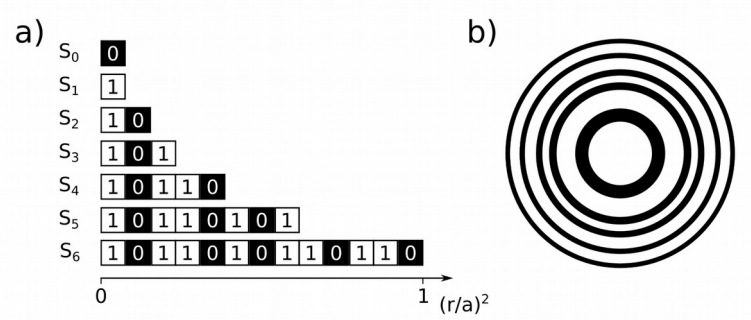

Fig. 1.4: a) Perfil radial cuadrático de una lente de Fibonacci binaria de amplitud, b) Transmitancia de la correspondiente lente de Fibonacci.

número mágico, un número irracional de valor $(1+\sqrt{5})/2$. A partir de la secuencia de Fibonacci, se pueden caracterizar, por ejemplo, desde la forma helicoidal en semillas [Fleming02] hasta el comportamiento de diferentes sistemas dinámicos [Linage06].

De forma similar a los números de Fibonacci, podemos generar una cadena de elementos partiendo de las semillas descritas por S_0={ ■ } y S_1={ □ }. El *i*-ésimo elemento de la cadena de Fibonacci vendrá dado por la concatenación de los anteriores, $S_i = \{S_{i-1}\, S_{i-2}\}$, con i>1, por lo que S_2={ □■ }, S_3={ □■□ }, S_4={ □■□□■ }, y así sucesivamente (ver Fig. 1.4a).

En el ámbito de las estructuras difractivas aperiódicas, las lentes basadas en la cadena de Fibonacci [Monsoriu03], se caracterizan por ser bifocales, siendo la relación de sus correspondientes distancias focales igual a la proporción áurea. En la Fig. 1.4a se muestra la transmitancia de una lente binaria de amplitud basada en la secuencia de Fibonacci. También se han propuesto lentes tipo kinoform basadas en esta secuencia [Ferrando14]. Al igual que las lentes binarias, las lentes kinoform de Fibonacci son bifocales, pero con una considerable mejora en su eficiencia en difracción, apodizando los focos de orden superior.

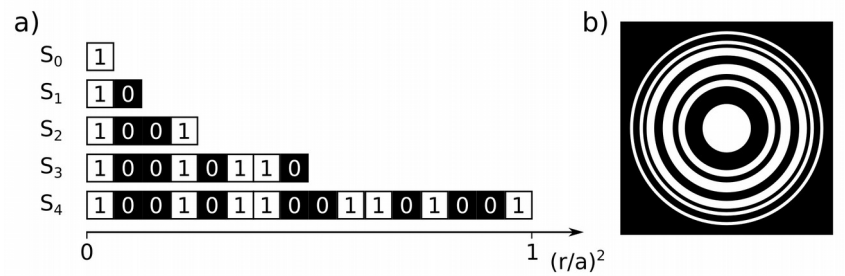

Fig. 1.5: a) Perfil radial cuadrático de una lente de Thue-Morse. b) Transmitancia de la correspondiente Thue-Morse de orden 4.

Combinando las lentes de Fibonacci con máscaras de fase helicoidales [Calatayud13a], se pueden generar dobletes de vórtices ópticos que posteriormente podrán ser utilizados en el diseño de nuevas trampas ópticas. Además de atrapar y manipular micropartículas, los vórtices ópticos también se utilizan en el control de bombas ópticas mesoscópicas en sistemas de microfluidos [Ladavac04], así en como actuadores y medidores en sistemas micro-mecánicos [Bishop03]. En los lentes-vórtice de Fibonacci, las distancias de los dos vórtices ópticos al plano de la lente también viene dada por la proporción áurea.

Lentes de Thue-Morse

La secuencia de Thue-Morse es una de las distribuciones aperiódicas consideradas en el diseño de lentes difractivas antes de iniciar el proyecto de Tesis Doctoral. Esta secuencia se define a partir de una semilla S_0={ □ }.

Cada elemento de la secuencia se obtiene de forma iterativa reemplazando □→□■ y ■→■□, por lo que S_1={ □■ }, S_2={ □■■□ }, S_3={ □■■□■□□■ }, … (ver Fig. 1.5a). Esta secuencia ha sido aplicada en diferentes ámbitos, como son los cristales fotónicos [Tsao14], láminas de grafeno [Huang13],

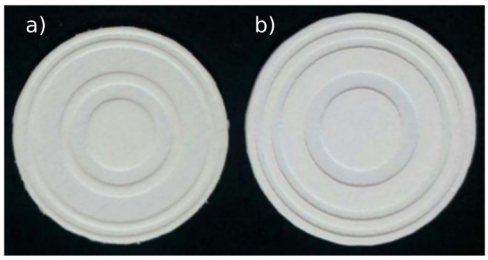

Fig. 1.6: Lentes difractivas de THz impresas en 3D: a) PZ fractal, b) PZ Fibonacci.

metamateriales [Monsoriu07] y pozos cuánticos [Hsueh14], entre otros.

Una lente difractiva basada en la secuencia determinista Thue-Morse [Ferrando15], reúne las ventajas de la PZF caracterizada por una escasa aberración cromática y de la lente de Fibonacci que genera dos focos a lo largo del eje óptico. Es decir, una lente de Thue-Morse genera dos focos autosimilares a lo largo del eje óptico.

Lentes de THz

En múltiples aplicaciones en el campo de los THz se requieren dispositivos pasivos para guiar y manipular esta radiación, incluyendo filtros [Wilk09], lentes [Scherger11a, Scherger11b] y guías de onda [Astley10]. Para estas aplicaciones es muy importante que elementos ópticos como espejos y lentes tengan un alto nivel de eficiencia, ya que para esta radiación electromagnética hay una deficiencia de fuentes de alta potencia y sensores con alta sensibilidad. Por lo tanto, al igual que en el rango visible, lentes difractivas optimizadas con secuencias aperiódicas son de especial interés en aplicaciones de THz.

Utilizando tecnología de impresión 3D, se han construido prototipos de PZF y lentes de Fibonacci para THz [Furlan16]. Estas lentes (ver Fig. 1.6) han sido caracterizadas tanto teórica como experimentalmente, demostrando que las propiedades de las lentes difractivas aperiódicas son perfectamente escalables al rango de los THz.

Objetivos

En el presente proyecto de Tesis Doctoral se pretende profundizar en el estudio de secuencias aperiódicas con el fin de explotar sus posibilidades en el contexto de la óptica difractiva. Adicionalmente, se abordará el diseño de lentes difractivas en el rango de los THz. De modo más detallado, los objetivos concretos de la Tesis se muestran a continuación:

1. Diseño y optimización de elementos ópticos difractivos multifocales binarios de amplitud o fase basados en nuevas secuencias aperiódicas deterministas, tales como las funciones de Walsh y la secuencia de *m*-bonacci.

2. Diseño y modelización de elementos ópticos difractivos con diferente carga topológica que genere nuevas secuencias de vórtices a lo largo del eje óptico, permitiendo así el diseño de nuevas trampas ópticas.

3. Diseño, construcción de prototipos y caracterización experimental de diferentes lentes difractivas en el rango de los THz. Estos prototipos se realizarán mediante tecnología de impresión 3D.

1.2 Estructura de la Tesis

Esta Tesis Doctoral se ha estructurado en la modalidad de compendio de publicaciones. Cada una de ellas puede ser leída de

forma autónoma, aunque siguen una clara línea argumental de forma que la unión de todas ellas constituye un único trabajo. Así pues, los capítulos desarrollados en esta Tesis son los siguientes:

1. Introducción general.
2. Publicaciones.
   - 2.1. Fractal light vortices.
   - 2.2. Diffractive *m*-bonacci lenses.
   - 2.3. Multiple-plane image formation by Walsh zone plates.
   - 2.4. Terahertz sieves.
   - 2.5. Multiplexing THz vortex beams with a single diffractive 3D printed lens.
3. Discusión general de resultados.
4. Conclusiones.

En el **primer capítulo**, como hemos visto, se incluye una introducción general del contenido de la Tesis y se describe brevemente el estado del arte relacionado con las placas zonales periódicas y aperiódicas. Además, en este capítulo se definen los objetivos concretos de la Tesis, se especifica la estructura de la presente memoria, el hilo común que siguen las publicaciones, y la calidad e impacto las mismas.

En el **segundo capítulo** se presentan las 5 publicaciones realizadas. La primera es un capítulo de un libro centrado en lentes-vórtice basadas en geometrías fractales. En la segunda y tercera publicación se presentan nuevas lentes difractivas aperiódicas cuyas transmitancias se definen a partir de las funciones de Walsh y la secuencia *m*-bonacci. Finalmente, en las dos últimas publicaciones se muestra tanto el diseño, construcción y caracterización experimental de lentes difractivas aplicadas a la focalización de haces de THz.

La **primera publicación**, “Fractal Light Vortices”, es el capítulo 10 del libro titulado “Vortex Dynamics and Optical Vortices”, publicado por la editorial InTech. Se trata de una editorial internacional competitiva de acceso abierto. El libro se encuentra indexado en el Book Citation Index y otras bases de datos científicas. El capítulo en cuestión ya ha recibido dos citas desde su reciente publicación [Zheng18, Ji18] según la base de datos del Web of Science. El libro, en su conjunto, aborda tanto teórica como experimentalmente una serie de trabajos relacionados con la dinámica de vórtices ópticos. El capítulo 10, “Fractal Light Vortices” constituye un artículo de revisión escrito por invitación de la editorial que resume todos los resultados obtenidos en el diseño y caracterización de lentes-vórtices basadas en geometrías fractales.

La **segunda publicación** titulada “Diffractive *m*-bonacci lenses” se ha publicado en Optics Express, una revista de alto prestigio internacional en el área de óptica. Esta revista tiene un factor de impacto de 3.31 en el JCR del 2016 y se ubica en el cuartil Q1 (17/92) en la categoría de OPTICS. En este artículo se presenta una nueva lente binaria de amplitud, cuyo perfil radial está definido por las secuencias de Tribonacci y Tetranacci, generalizando así los resultados previamente obtenidos con las lentes de Fibonacci. Estas lentes difractivas aperiódicas producen un desdoblamiento del foco principal respecto a la lente periódica equivalente. La relación entre las correspondientes distancias focales viene dada por la proporción áurea generalizada.

La **tercera publicación** denominada “Multiple-plane image formation by Walsh zone plates” se encuentra actualmente en proceso de revisión en una revista internacional de prestigio en en ámbito de la óptica. En este trabajo se aplica la función radial de Walsh para el diseño de una lente binaria de amplitud capaz de focalizar en cuatro puntos del eje de propagación. Por lo tanto,

como lente difractiva cuatrifocal podría tener especial interés en el diseño de nuevas lentes oftálmicas multifocales.

La **cuarta publicación**, “THz Sieves”, se ha publicado en la revista IEEE Transactions on Terahertz Science and Technology. Esta revista tiene un factor de impacto de 1.63 en el JCR del 2016 y se ubica en el cuartil Q1 en la categoría de OPTICS (20/92). En este artículo se incluye el diseño y caracterización experimental de cribas de fotones en el rango de los THz fabricadas mediante técnicas de impresión 3D.

La **quinta publicación**, “Multiplexing THz vortex beams with a single diffractive 3D printed lens”, se encuentra en proceso de revisión en una revista de alto prestigio internacional en el ámbito de la óptica. En este trabajo se propone el multiplexado de vórtices en el rango de THz mediante la construcción de prototipos de lentes-vórtice impresos en 3D y en los que se combinan dos cargas topológicas en una misma lente.

Capítulo 2

Publicaciones

2.1 Fractal Light Vortices

Abstract

Vortex lenses produce special wavefronts with zero-axial intensity, and helical phase structure. The variations of the phase and amplitude of the vortex produce a circular flow of energy that allows transmitting orbital angular momentum. This property is especially in optical trapping, because due to the orbital angular momentum of light, they have the ability to set the trapped particles into rotation. Vortex lenses engraved in diffractive optical elements have been proposed in the last few years. These lenses can be described mathematically as a two-dimensional (2D) function, which expressed in polar coordinates are the product of two different separable one-dimensional (1D) functions: One, depends only on the square of radial coordinate, and the other one depends linearly on the azimuthal coordinate and includes the topological charge. The 1D function that depends on the radial coordinate is known as a zone plate. Here, vortex lenses, constructed using different aperiodic zone plates, are reviewed. Their optical properties are studied numerically by computing the intensity distribution along the optical axis and the transverse diffraction patterns along the propagation direction. It is shown that these elements are able to create a chain of optical traps with a tunable separation, strength and transverse section.

Introduction

Vortex lenses (VLs) produce special wavefronts with zero-axial intensity, and helical structure with undefined phase in the vortex centre. These structures, called optical vortices

[Desyatnikov15, Roux04, Grier03], constitute an intriguing and growing area of research that combines fundamental theoretical aspects and novel applied technologies. A fundamental property of vortices is the conservation of the topological charge which is defined as the 2π module of the total change of the phase along a closed curve surrounding the vortex centre. The variations of the phase and amplitude of the vortex produce a circular flow of energy that allows to carry orbital angular momentum [Allen99, Bekshaev08]. This property is useful for several applications, such as in astrophysics [Lee06, Swartzlander08], transmission of information [Gibson04, Bouchal04], microscopy [Spektor08], laser engraving [Turitsyn07] and especially in optical traps [Gahagan96, Garcés-Chávez02, Reicherter99, Ladavac04, Friese01], because due to the orbital angular momentum of light, they have the ability to set the trapped particles into rotation.

Several methods have been proposed to obtain optical vortices [Grier03, Allen99, Masajada01, Yang14, Brasselet09, Curtis02] being spiral phase plates (i.e. lenses with a linear phase dependence on the azimuthal angle) and diffractive optical elements (DOEs) probably the most frequent approach. In fact, due to its simplicity, they can be employed in multiple applications. In particular, zone plates (ZPs) have found a great number of new applications in the last few years [Ojeda-Castaneda96]. A standard amplitude ZP consists of a series of concentric circular rings of equal area, with alternating transmitting and absorbing zones. This means that along the square of the radial coordinate, a ZP can be thought as a periodic structure. The focusing effect is created by the constructive interference of waves passing through this structure.

On the other hand, in recent years different non-periodic and quasi-periodic sequences [Maciá06] have been also employed to design new types of ZPs with curious physical properties. Fractal zone plates (FrZPs) [Saavedra03, Furlan07], Fibonacci zone plates

(FiZPs) [Monsoriu13a, Ferrando14], Thue-Morse zone plates (TMZPs) [Ferrando15a] and some variations of these basic designs are representative examples [Giménez10a, Giménez06, Giménez10b].

FrZPs are characterized by its fractal structure along the square of the radial coordinate that produce multiple foci along the optical axis which are defined by the self-similar Fourier spectrum of the fractal pupil function [Saavedra03]. These lenses produce a main focus surrounded by numerous secondary foci, which together result in a compound focal volume. It has been demonstrated that these self-similar foci produce reduction of the chromatic aberration under wideband illumination and increase of depth of field [Furlan07].

FiZPs are bifocal ZPs with their foci located at certain axial positions given by the Fibonacci numbers, being the ‘golden mean’, the ratio of the two focal distances [Monsoriu13a]. As the name indicates, these lenses are designed following an aperiodic structure generated by the Fibonacci sequence. The focusing and imaging capabilities of Fibonacci lenses have been experimentally demonstrated under monochromatic illumination [Ferrando14]; however, these lenses are affected by the same limitations of conventional ZPs when broadband illumination is considered, since the twin foci are not self-similar.

TMZPs are based on the deterministic Thue-Morse sequence, which results in a combination of the FrZP and FiZP. For this reason, this new family of aperiodic ZPs combines the advantages of fractal ZPs (reduction of the chromatic aberration) and Fibonacci ZPs (bifocusing along the optical axis) [Ferrando15a].

In this chapter, the combination of a vortex lens and ZPs, constructed using different aperiodic sequences, in a single element is considered. Their optical properties are investigated

numerically and experimentally. The focusing properties of different combinations of FZPs and vortex lenses are studied by computing the intensity distribution along the optical axis and the transverse diffraction patterns along the propagation direction. The diffracted field of these vortex lenses was obtained numerically within the Fresnel approximation

We emphasize that these elements are able to create a chain of optical traps along the optical axis with a tunable separation, strength and transverse section. We discuss the influence of the topological charge on the irradiance propagation and also we investigate the variation of the angular momentum provided by the doughnut-shaped foci.

An optical set-up was implemented to obtain experimental results in which the VLs were registered in a spatial light modulator (SLM).

We have shown that our VLs are able to generate multiple-plane optical trappings with a volumetric extension. In this sense, they are superior to conventional vortices, whose extension is limited to the depth of focus of the beam.

Basic theory

The transmittance of a VL can be expressed as the product of two factors being the first one associated to a given ZP, which has only a radial dependence, and the other one corresponding to a vortex lens with a linear phase dependence on the azimuthal angle θ.

A ZP can be realized from a one-dimensional (1D) compact-supported periodic function $q(\zeta)$ as shown in Fig.2.1, where $\zeta=\left(\frac{r}{a}\right)^2$ is the normalized square radial coordinate and a is the external radius of the outermost ring. Therefore, in a binary ZP,

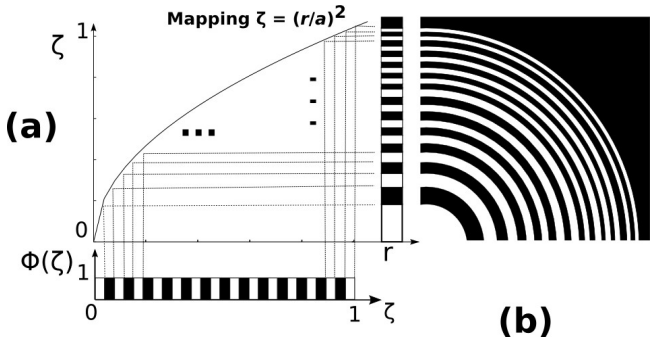

Fig. 2.1. Schematic representation of the geometrical construction of a ZP from a periodic binary function. (a) Variable ζ mapped as function of r 2 . (b) Layout of zones on ZP lens.

every pair of opaque and transparent zones conforms a period. The area of each period is constant over all the ZPs.

In a similar way, the aperiodic zone plates that we consider from now on can be constructed by replacing the periodic function $q(\zeta)$ by either the Cantor function, the Fibonacci sequence or the Thue-Morse sequence. In fact, when designing VL, each of these sequences can be used to define the transmission generating function $q(\zeta)$ with compact support on the interval $\zeta\in[0,1]$.

This interval is partitioned in 2S sub-intervals of length $dS=\frac{1}{2S}$ and the transmittance value $t_{S,j}$, which takes at the *j*-th sub-interval, is associated to the value of the element $D_{S,j}$, being $t_{S,j}=1$ for the transparent zones and $t_{S,j}=0$ for the opaque zones.

To study the focusing properties of VLs, we compute the irradiance provided by the transmittance of each lens described in general terms as

$$t(\zeta,\theta_0)=q(\zeta)\exp(\mathrm{i}m\theta_0) \tag{1}$$

where the azimuthal dependence is characterized by the topological charge *m*. We consider monochromatic plane wave

illumination of wavelength λ. Thus, within the Fresnel approximation the irradiance function is given by

$$I(u,v;\theta)=u^2\left|\int_0^1\int_0^{2\pi} t(r,\theta_0)\exp(-i2\pi u\zeta)\exp[i4\pi u v\zeta^{1/2}\cos(\theta-\theta_0)]d\zeta\, d\theta_0\right|^2 \quad (2)$$

where $u=\frac{a^2}{2\lambda z}$ is the dimensionless reduced axial coordinate and $v=\frac{r}{a}$ is the normalized transverse coordinate [Saavedra03]. By using Eq. (1) and taking into account that

$$\begin{aligned}\int_0^{2\pi} t(\zeta,\theta_0)\exp(-2\pi u\zeta)\exp\left[i4\pi u v\zeta^{1/2}\cos(\theta-\theta_0)\right]d\theta_0 \\ =2\pi\exp\left[\mathrm{im}\left(\theta+\frac{\pi}{2}\right)\right]J_m\left(4\pi u v\zeta^{1/2}\right)\end{aligned} \quad (3)$$

Equation 2 is reduced to

$$I(u,v)=4\pi^2u^2\left|\int_0^1 q(\zeta,\theta_0)\exp(-2\pi u\zeta)J_m\left(i4\pi u v\zeta^{1/2}\right)d\zeta\right|^2 \quad (4)$$

$J_m(\,)$ being the Bessel function of the first kind of order m.

Fractal vortex lenses

Two different results were independently obtained by combining spiral phase plates with FrZP to produce a sequence of focused optical vortices along the propagation direction. In Ref. [Tao06], the spiral fractal zone plate is generated as a phase-only FrZP modulated by helical phase structure. Another design of spiral phase plate based on a *blazed* FrZP, the devil's lens [Furlan09], was proposed to improve diffraction efficiency of a spiral FrZP. A devil's lens has a characteristic surface relief along

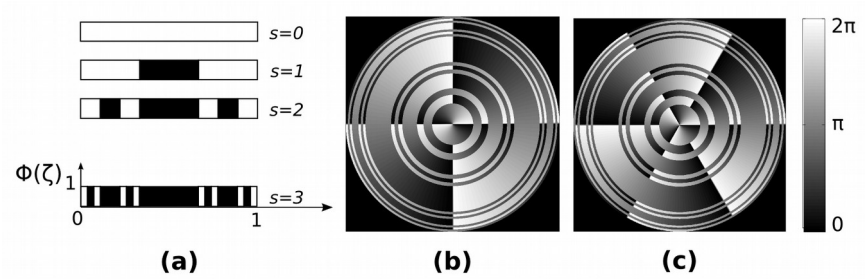

Fig. 2.2. FVL construction: (a) Diagrams of the generation of binary function for a FZP for N = 2 and several values of S. (b) FVL with m=2. (c) FVL with m=3. In this representation, open and filled segments correspond to phase values differing in π of the generating radially binary function.

the radial coordinate which is obtained using the devil's staircase function [Monsoriu07a]. It is because of its blazed profile that devil vortex lens has improved diffraction efficiency with respect to the spiral fractal zone.

The focal volume generated by Fresnel vortex lenses (FrVLs) results in a chain of vortices that could be used as versatile and very efficient optical tweezers because, in addition to rotating the trapped particles with high refractive index, other particles with a lower refractive index can be trapped in the vortex centre. The relative angular velocity of the particles at the different traps can be changed with different topological charges; the distances between the links of the chain can be modified with different values of S-parameter.

Following the same approach employed in Fig. 2.2, an FrVL is mathematically obtained by replacing the periodic sequence by a Cantor structure developed up to certain stage. Let us consider, for example, the triadic regular Cantor sequence. The construction procedure is shown in Fig. 2.2a. In the first stage, $S=1$, the segment is divided into three parts, and the middle one is removed. In the second stage, this slicing-and-removing process is repeated

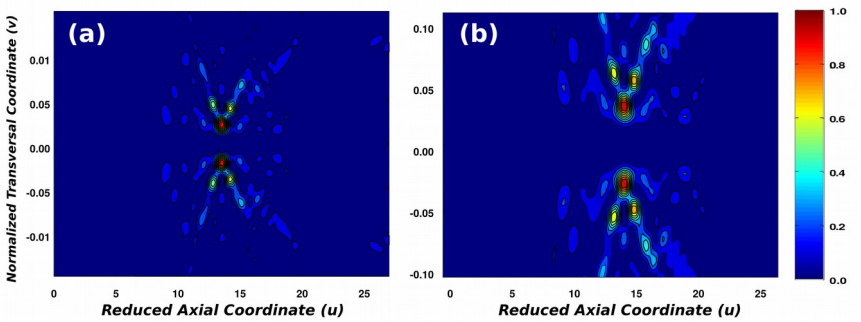

Fig. 2.3. Normalized irradiance contours for the FVL in Fig.1: (a) m = 2 and (b) m = 3.

in each one of the remaining two segments from the first stage. This process is repeated in the following stages. In mathematical terms, the FrVL transmittance function, for a given stage *S*, can be expressed by replacing the following generating function of the FrZP in Eq. (1) [Saavedra03]:

$$q(\zeta, S; N) = \prod_{i=1}^{S} \mathrm{rect}\left[\zeta^2 - 0.5\right] \mathrm{rect}\left\{ mod\left[\zeta^2 - 1 + \frac{1}{(2N-1)^i}, \frac{2}{(2N-1)^i} \right] \frac{(2N-1)^i}{2} \right\} \quad (5)$$

In which the transparent and opaque zones are replaced by pure phase zones differing in π for the design wavelength. In this equation, the function $mod(x, y)$ gives the remainder on division of *x* by *y*.

Typical results are shown in Fig. 2.2b for a fractal vortex lens with topological charge *m=2* and in Fig. 2.2c for a FVL with topological charge *m=3*.

By using expression (4), we have computed the irradiance provided by these FrVLs at transverse planes along the optical axis. The result is shown in Fig. 2.3.

As we mentioned, the diffraction efficiency of these FVLs can be improved by imposing ablazed profile to the radial

coordinate. This can be done by using the Cantor function, or devil's staircase, as a generating $q(\zeta)$ function [Furlan09, Furlan10]. The focusing properties of these FVL were experimentally analyzed in [Calatayud12]. It has been demonstrated that for multiple-plane optical trappings, they can generate a light beam with axially distributed optical vortices. The transverse patterns appearing along the propagation distance present several concatenated dough-nut modes as represented in Fig. 2.3.

Besides, the generation of multiple vortex distributions is of interest as demonstrated by the new methods that have been recently proposed to generate different two-dimensional (2D) and three-dimensional (3D) arrays of vortices. Different methods have been employed, such as interferometric techniques using Michelson or Mach-Zehnder interferometers [Vyas07] and Dammann gratings [García-Martínez12]. A simple method to obtain special arrays of vortices is possible by means of a reconfigurable spatial light modulator (SLM). In fact, the use of an SLM allowed the possibility to change in a simple way the characteristics of diffractive lenses, such as their focal length or their topological charge. The implementation of compound 3D optical vortex structures by means of an array of DVLs was reported in [Calabuig13] with numerical simulations and experimental results.

Fibonacci vortex lenses

Fibonacci vortex lenses (FiVLs) are constructed using the Fibonacci sequence [Maciá06]. This sequence has been also employed in the development of different photonic devices and applications [Maciá12], such as multilayers and gratings [Sah95], cryptography [Zhou12] and photonic crystals[Lusk01].

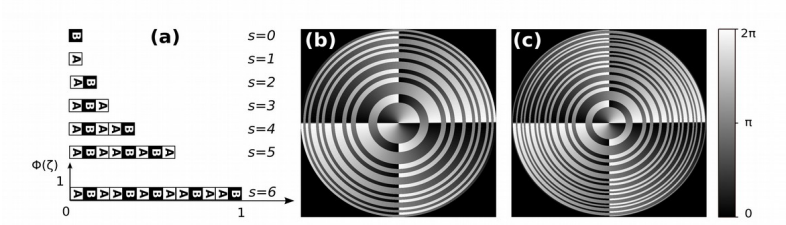

Fig. 2.4. FiVL construction: (a) Diagrams of the generation of binary function for an FiZP and several values of S. (b)FiVL with S=7 and m=2. (c) FiVL with S=8 and m=2. In this representation, open and filled segments correspond tophase values differing in π of the generating radially binary function.

The Fibonacci sequence is a set of ordered numbers, $F_j=\{0,1,1,2,3,5,8,13,21,...\}$, that are obtained following a simple rule: Starting with two elements (called seeds) $F_0=0$ and $F_1=1$, the following numbers of the sequence are obtained as $F_j+1=F_j+F_{j-1},(j=0,1,2,...)$. The ratio of two consecutive elements of the Fibonacci sequence approaches asymptotically an irrational number known as the golden mean: $\varphi=\lim_{j\to\infty}\frac{F_j}{F_{j-1}}=\left(\frac{1+\sqrt{(5)}}{2}\right)$. Fibonacci series and the golden mean have been ubiquitously observed in nature and on different scientific areas [Basin63, Garland87].

Based on the Fibonacci numbers, a binary Fibonacci sequence can also be generated with two seed elements, $S_1=\{A\}$ and $S_2=\{B\}$, as shown in Fig. 2.4a. Then, the next order of sequence is obtained simply as the concatenation of the two previous ones: $S_{j+1}=\{S_j,S_{j-1}\}$ for $j\geq 1$.

Consequently, $S_3=\{AB\}$, $S_4=\{ABA\}$, $S_5=\{ABAAB\}$, $S_6=\{ABAABABA\}$, and so on. It should be noted that the total number of elements of the order *j* sequence is F_{j+1} and that, for each *S*, two consecutive 'B' are separated by either one or two 'A'.

Each sequence can be used tobdefine the binary generating function for the radial phase distribution of the FiVL.

In our case, the function, $\Phi_j(\zeta)$, is defined in the domain [0,1], which is partitioned in F_{j+1} sub-intervals of length $1/F_{j+1}$. Therefore, the function $\Phi_j(\zeta)$ at the k_{th} sub-interval is either 0 or π if the value of the k_{th} element of the S_j sequence, S_{jk} is 'A' or 'B', respectively. Finally, after performing the coordinate transformation, $q(\zeta)=\left(\frac{r}{a}\right)^2$, the radial part of the transmittance is obtained as $q(\zeta)=\exp[i\Phi_j(\zeta)]$ as shown in Fig.2.1.

An FiVL is defined as a pure phase diffractive element whose phase distribution is given by $\Phi_{FVL}(\zeta,\theta_0)=\mathrm{mod}\,2\pi[\phi_j(\zeta)+m\theta_0]$. Thus, it combines the azimuthal phase variation that characterizes a vortex lens, with the radial phase distribution that is generated through the Fibonacci sequence. Fig.2.4b and Fig.2.4c shows the results for $S=7$ and $S=8$ for the topological charge $m=2$.

Compared with a Fresnel zone plates (which, we recall, can be considered periodic structures along the square radial coordinate ζ), it can be verified that if both have the same number of elements, F_j, but the position of some zones with different phase has been interchanged, the FiZP produces a focal splitting of the main focus of the Fresnel zone plate along the axis. Thus, an FVL with $m=0$ can be understood as two Fresnel zone plates interlaced [Monsoriu13b].

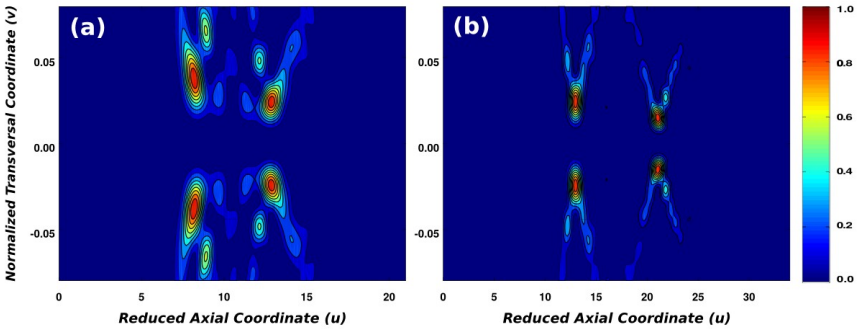

Fig. 2.5. Normalized irradiance contours for the FVL in Fig. 4: (a) FiVL with . (b) FiVL with S=7, m = 2. (b) FiVL with S = 8, m = 2.

The irradiances provided by the lenses are shown in Fig. 2.4. The result is shown in Fig. 2.5. The integrals were computed using Eq. (4) applying Simpson's rule with a step length 1/2000.

Note that FiVLs produce twin foci whose locations are coincident with the Fibonacci numbers. In fact, for S_8 FVLs, the first focus is located at $u_1=13=F_{J-1}$ and the other one at $u_2=21=F_J$. Moreover, the ratio of the focal distances satisfies $\frac{u_2}{u_1}\approx\varphi$. The diameter of these 'twin' vortices provided by FiVLs is related by the golden mean [Calatayud13], and the diameter of the rings increases proportionally with the topological charge.

Thue-Morse vortex lens

The Thue-Morse sequence [Maciá06] is also a binary sequence in which each element is obtained with the previous one by appending to it its Boolean complement. This sequence has been applied in several branches of Physics, as, for example, in the context of photonic crystals [Tsao14], quantum wells [Hsueh14], metamaterials [Monsoriu07b] and graphene superlattices [Huang13].

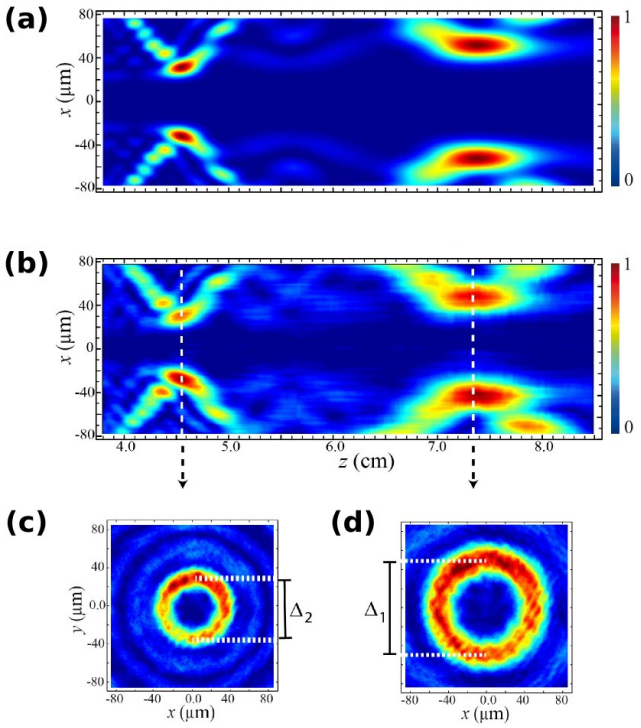

Fig. 2.6. Longitudinal irradiance of different planes produced by FiVL with (a) theoretical results, (b)experimental results. (c and d) Transverse irradiance at the planes indicated by the arrows.

The characteristic function $q(\zeta)$ corresponding to the Thue-Morse sequence is constructed defining a seed $D_0 = A$ from which the following elements in the sequence are obtained by replacing A by AB and B by BA. In this way, $D_1 = AB$, $D_2 = ABB$, $D_3 = BBABAAB$, $D_4 = ABBABAABBAABABBA$, and so on. Fig. 2.7a shows the geometrical construction of the TM sequence up to order $S = 4$. When designing Thue-Morse vortex lens (TMVL), each D_i can be used to define the transmission function $q(\zeta)$ with

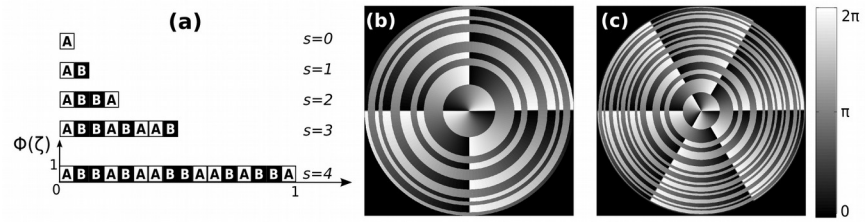

Fig. 2.7. TMVL construction: (a) Diagrams of the generation of binary function $q(\zeta)$ *for TMVL and several values of S. (b)TMVL S = 4 with m = 2. (c) TMVL S = 5 with m = 3. In this representation, open and filled segments correspond to phase values differing in* $q(\zeta)$ *of the generating radially binary function.*

compact support on the interval $\zeta\in[0,1]$. This interval is divided in 2S sub-intervals of length $dS=1/2S$, where the transmittance, $t_{S,j}$, of the *j*-th sub-interval is associated to the element $D_{S,j}$, as $t_{S,j}=1$ when $D_{S,j}$ is 'A', and $t_{S,j}=0$ when $D_{S,j}$ is 'B'. Note that like a conventional ZP the period of a TMZP is $pS=2dS$, where the position of transparent/opaque zones has been interchanged. In mathematical terms, the transmittance function, $q(\zeta)$, can be written as

$$q(\zeta)=\sum_{j=1}^{2^S} t_{S,j}\,\mathrm{rect}\left[\frac{\zeta-(j-0.5)d_S}{d_S}\right] \tag{6}$$

Fig. 2.8 shows the axial irradiance provided by TMVLs of orders $S=4$ and $S=5$. Note that the Thue-Morse ZP produces a symmetrical splitting of the first-order focus. This zero irradiance in the middle is due to the destructive interference generated by the two conjugated parts of the lens. In this way, like FiVLs, TMVLs are bifocals, but they produce a sequence of secondary foci around each main focus that have a fractal structure. In fact, it has been shown that irradiance provided by these lenses with topological charge $m=0$ is self-similar [Ferrando15b], that is, the irradiance distribution corresponding to a TMVL of order S is a modulated

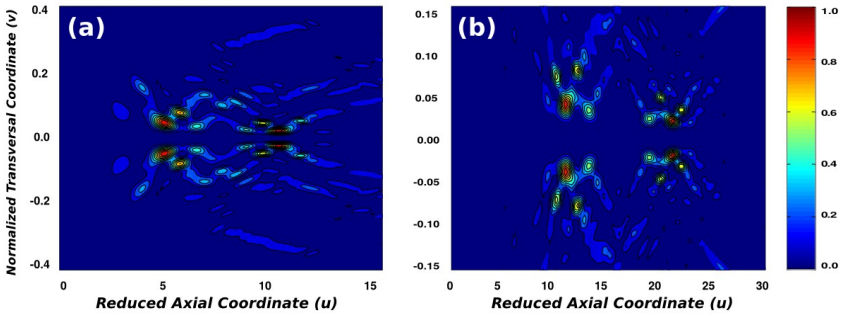

Fig. 2.8. Normalized irradiance contours for the TMVL in Fig. 7: (a) S = 4 with m = 2. (b) S = 5 with m = 3.

version of the irradiance distribution corresponding to the previous stage, $S-1$, magnified by a factor 2

In Fig.2.8, we represent the axial irradiances provided by the TMVLs represented in Fig. 2.7. It can be seen that TMVLs produce a bifocal structure with fractal characteristic. It can also be observed that the diameters of these 'twin' vortices provided are proportional to the topological charge.

Experimental results

For the experimental study of the properties of FVLs, we implemented the experimental set-up shown in Fig. 2.9, where the aperiodic VLs were experimentally implemented in a programmable spatial light modulator. The static aberrations caused by the SLM display were characterized with a Shack-Hartmann wavefront sensor, and then compensated as detailed elsewhere [Calatayud12]. The vortex-lens performance was studied computing the diffraction patterns along different planes along the optical axis.

The proposed ZPs were recorded on a spatial light modulator (Holoeye PLUTO, eight-bit grey-level, pixel size 8 μm and

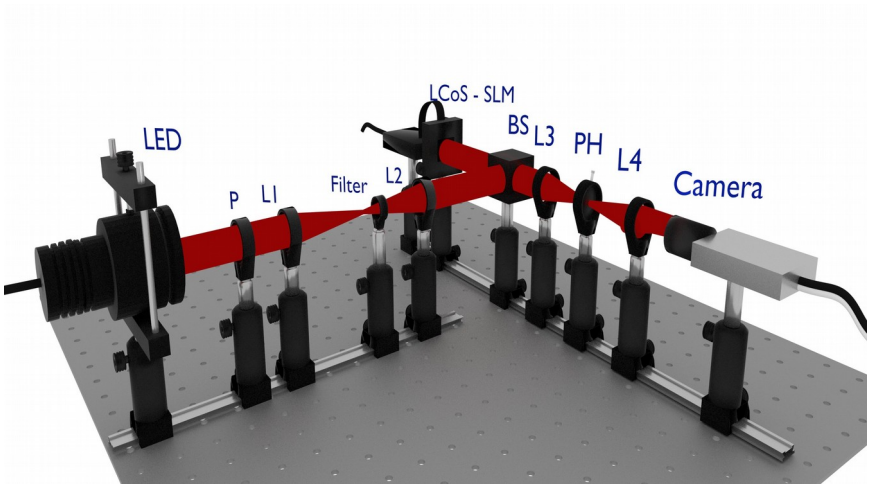

Fig. 2.9. Experimental set-up for characterization and measuring vortices for FVLs.

resolution equal to 1920 × 1080 pixels), calibrated for a 2π phase shift at λ = 633 nm operating in phase-only modulation mode.

A linear phase grating was superposed to the diffractive lenses on the SLM to avoid the specular reflection and the pixelated structure of the SLM. This linear phase was compensated by an appropriate tilt of the SLM. A pin hole (PH) was used to filter high diffraction orders. A scaled image of the lens was achieved at the L3 lens focal plane (exit pupil).

A collimated He-Ne laser beam (λ = 633 nm) was sent to the SLM and the diffracted field was registered with an eight-bit grey-level, charge-coupled device (CCD) camera (EO-1312M 1/2" CCD Monochrome USB Camera, pixel pitch of 4.65 μm, 1280 × 1024 pixels) through a microscope objective (10× Zeiss Plan-Apochromat). The microscope and the CCD were mounted on a translation stage (Thorlabs LTS 300, range: 300 mm and 5 μm precision). The computed and experimental irradiances produced by an S_8 FiVL with $m=6$ are shown in Fig. 2.6.

As predicted by the theoretical analysis (Fig. 2.6a), the axial localization of the focal rings depends on the Fibonacci numbers F_j and F_{j+1}, and such focal distances satisfy the following relationship: $\frac{f_1}{f_2}=\frac{F_j}{F_{j-1}}\approx\Phi$. The diameter of the rings also satisfies $\frac{\Delta_1}{\Delta_2}\approx\Phi$.

Conclusions.

A new family of fractal aperiodic VLs with interesting focusing and imaging capabilities has been presented. The transverse patterns appearing along the propagation distance present several concatenated doughnut modes. The ability of these VLs to produce multiple vortex tweezers has been demonstrated. In fact, it was found that contrary to conventional spiral zone plate, which produces a single vortex, each member of this family generates a delimited chain of vortices that are axially distributed. The distances between the links of the chain depend on the level *S* of the generating function and the radii of the doughnuts increase with the topological charge. Additionally, the multifocal nature of the lens, resulting from its fractal structure along the radial coordinate, could provide a high depth of field, especially with wide band sources.

In the case of FrVL (i.e. Cantor and Devil's VLs), the evolution of the axial irradiance replicates the fractality of the pupil. The orbital angular momentum in each link on the chain also depends on the topological charge but it is nearly independent of its axial location.

Our analysis demonstrated the possibility of simple design procedure arrays of VLs with any desired range of topological charge. As each individual VL can be understood as a light gear capable of driving microstructures around its circumference,

applications involving particle transfer and manipulation could be foreseen.

On the other hand, FiVLs and TMVLs are intrinsically bifocal vortex lenses. It was shown that they produce twin optical vortices along the axial coordinate. The positions of both foci depend on the two incommensurable periods of the Fibonacci sequence in which the lenses are based. Moreover, the evolution of the irradiance along the propagation axis reproduces the fractality of the lens [Furlan10]. The diameter of these chains of vortices is proportional to the topological charge, and their ratio is close to the golden mean. The volumetric distribution of the diffracted field generated by FiVLs was assessed experimentally using an SLM. An excellent agreement was found between the experimental results and the theoretical predictions.

The peculiar focal volume obtained with DVLs could be exploited as versatile and efficient optical tweezer, because it can also trap low-index particles in the zero-intensity axial zone of the doughnut and at the same time can exert a torque on small objects having a high refraction index. The distances between the links of the vortex chain can be modified with the level S of the generating function and relative angular velocity of the particles at the trap depends on the topological charge of the vortex.

Another potential application of these optical vortices arises in X-ray microscopy where its azimuthal component can be used for detecting the phase component of objects with complex index of refraction since it acts as a Hilbert phase filter. This feature is especially useful in the case of biological specimens to provide enhanced contrast.

TMVL produces a couple of self-similar vortex located symmetrically one at each side of the focus of the equivalent periodic VL. Therefore, under broadband illumination, a TMVL produces a pair of images with an extended depth of field and a

strong reduction in the chromatic aberration. In this way, TMVLs combine the characteristics of FrVLs and FiVLs and could be used in multiple applications including spectral domain optical coherence tomography (OCT) and X-ray microscopy [35].

Finally, it should be mentioned that all the aperiodic VLs here presented admit fractional topological charges that break down the symmetry of the foci and produce chains of anisotropic vortex foci.

Acknowledgements.

This work was founded by the Ministerio de Economía y Competitividad FEDER (GrantDPI2015-71256-R), and by Generalitat Valenciana (PROMETEOII-2014-072), Spain.

Federico Machado acknowledges support from the MayaNet - Erasmus Mundus Partnership552061-EM-1-2014-1-IT-ERA MUNDUS-EMA21 (2014-0872/001-001).

References

[Allen99] L. Allen, M. J. Padgett y M. Babiker, “The orbital angular momentum of light”, *Progress in Optics* **39**, 291–372 (1999).

[Basin63] S. L. Basin, “The Fibonacci sequence as it appears in nature”, *Fibonacci Quarterly* **1**, 53–56(1963).

[Bekshaev08] A. Bekshaev, M. Soskin y M. Vasnetsov, *Paraxial Light Beams with Angular Momentum*, Nova Publishers (2008)

[Bouchal04] Z. Bouchal y R. Čelechovský, “Mixed vortex states of light as information carriers”, *New Journal of Physics* 6, 1-15 (2004).

[Brasselet09] E. Brasselet, N. Murazawa, H. Misawa y S. Juodkazis, “Optical vortices from liquid crystal droplets”, *Physical Review Letters* **103**, 103903 (2009).

[Calabuig13] A. Calabuig, S. Sánchez-Ruiz, L. Martínez-León, E. Tajahuerce, M. Fernández-Alonso, W. D. Furlan, J. A Monsoriu, y A. Pons-Martí, “Generation of programmable 3D optical vortex structures through devil’s vortex-lens arrays", *Applied Optics* **52**, 5822–5829 (2013).

[Calatayud12] A. Calatayud, J. A. Rodrigo, L. Remón, W. D. Furlan, G. Cristóbal y J. A. Monsoriu, “Experimental generation y characterization of Devil’s vortex-lenses”, *Applied Physics B* **106**, 915–919 (2012).

[Calatayud13b] A. Calatayud, V. Ferrando, L. Remón, W. D. Furlan, y J. A. Monsoriu, “Twin axial vortices generated by Fibonacci lenses", *Optics Express* **21**, 10234–10239 (2013).

[Curtis02] J. E. Curtis, A. K. Brian y D. G. Grier, “Dynamic holographic optical tweezers”, *Optics Communications* **207**, 169-175 (2002).

[Desyatnikov15] A. Desyatnikov, Y. Kivshar y L. Torner, “Optical vortices y vortex solitons”, *Progress in Optics* **47**, 291–391 (2005).

[Ferrando14b] V. Ferrando, A. Calatayud, P. Andrés, R. Torroba, W. D. Furlan, y J. A. Monsoriu, “Imaging properties of Kinoform Fibonacci lenses", *IEEE Photonics Journal*. **6**, 6500106 (2014).

[Ferrando15] V. Ferrando, F. Giménez, W. D. Furlan, y J. A. Monsoriu, “Bifractal focusing y imaging properties of Thue-Morse Zone Plates", *Optics Express* 23, 19846–19853 (2015)

[Friese01] M. Friese, H. Rubinsztein-Dunlop, J. Gold, P. Hagberg y D. Hanstorp, “Optically driven micromachine elements”, *Applied Physics Letters* **78,** 547–549 (2001).

[Furlan07] W. D. Furlan, G. Saavedra, y J. A. Monsoriu, “White-light imaging with fractal zone plates", *Optical Letters* **32**, 2109–2111 (2007)

[Furlan09] W. D. Furlan, F. Giménez, A. Calatayud y J. A. Monsoriu, “Devil’s vortex-lenses”, *Optics Express* **17**, 21891–21896 (2009)

[Furlan10] W. D. Furlan, F. Giménez, A. Calatayud, L. Remón y J. A. Monsoriu, “Volumetric multiple optical traps produced by Devil's lenses”, *Journal of the European Optical Society-Rapid Publications* **5**, 10037s (2010).

[Gahagan96] K. T. Gahagan y G. A. Swartzlander, “Optical vortex trapping of particles”, *Optics Letters* **21**, 827 (1996)

[Garcés-Chávez02] V. Garcés-Chávez, K. Volke-Sepulveda, S. Chávez-Cerda, W. Sibbett y K. Dholakia, “Transfer of orbital angular momentum to an optically trapped low-index particle”, *Physics Review A* **66**, 063402 (2002)

[García-Martínez12] P. García-Martínez, M. M. Sánchez-López, J. A. Davis, D. M. Cottrell, D. Sy e I. Moreno, “Generation of Bessel beam arrays through Dammann gratings”, *Applied Optics* **51**, 1375–1381 (2012).

[Garland87] Garly T. H., *Fascinating Fibonaccis: Mystery y Magic in Numbers*, Dale Seymour Publications (1987).

[Gibson04] G. Gibson, J. Courtial, M. Padgett, M. Vasnetsov y V. Pasco, “Free-space information transfer using light beams carrying orbital angular momentum”, *Optical Express* **12**, 5448-5456 (2004).

[Giménez06] F. Giménez, J. A. Monsoriu, W. D. Furlan, y A. Pons, “Fractal photon sieve", *Optics Express* **14**, 11958–11963 (2006).

[Giménez10] F. Giménez, W. D. Furlan, A. Calatayud, y J. A. Monsoriu, “Multifractal zone plates", *Journal of the Optical Society of America A* **27**, 1851–1855 (2010)

[Grier03] D. G. Grier, “A revolution in optical manipulation”, **424**, 810–816 (2003).

[Hsueh14] W. J. Hsueh, C. H. Chang y C. T. Lin, “Exciton photoluminescence in resonant quasi-periodic Thue-Morse quantum wells”, *Optical Letters* **39**, 489–492 (2014).

[Huang13] H. Huang, D. Liu, H. Zhang y X. Kong, “Electronic transport y shot noise in Thue-Morse sequence graphene superlattice”, *Applied Physics* **113**, 043702 (2013).

[Ladavac04] K. Ladavac y D. Grier, “Micromechanical pump assembled y driven by holographic optical vortices”, *Optical Express* **12**, 1144–1149 (2004).

[Lee06] J. H. Lee, G. Foo, E. G. Johnson y G. A. Swartzlander, “Experimental verification of an optical vortex coronagraph”, *Physics Review Letters* **97**, 053901(2006).

[Lusk01] D. Lusk, I. Abdulhalim y F. Placido, “Omnidirectional reflection from Fibonacci quasi-periodic one-dimensional photonic crystal. Optics Communications”, **198**, 273–279 (2001).

[Maciá06] E. Maciá, “The role of aperiodic order in science and technology”, *Reports on Progress in Physics* **69**, 397-441 (2006).

[Maciá12] E. Maciá, “Exploiting aperiodic designs in nanophotonic devices”. *Reports in Progress on Physics* **75**, 1–42 (2012).

[Masajada01] J. Masajada y B. Dubik, “Optical vortex generation by three plane wave interference”, *Optics Communications* **198,** 21–27 (2001).

[Monsoriu07a] J. A. Monsoriu, W. D. Furlan, G. Saavedra y F. Giménez, “Devil’s lenses”, Optics Express **15**, 13858–13864 (2007).

[Monsoriu07b] J. A. Monsoriu, R. A. Depine y E. Silvestre, “Non-Bragg by gaps in 1D metamaterial aperiodic multilayers”, *Optics Express* **2**, 07002 (2007).

[Monsoriu13] J. A. Monsoriu, A. Calatayud, L. Remón, W. D. Furlan, G. Saavedra, y P. Andrés, “Bifocal Fibonacci diffraction lenses", *IEEE Photonics Journal* **5**, 3400106 (2013).

[Ojeda-Castaneda96] J. Ojeda-Castaneda y C. Gomez-Reino, “Selected Papers on Zone Plates”, *SPIE Optical Engineering Press* **MS128**, 512-518 (1996).

[Reicherter99] M. Reicherter, T. Haist, E. Wagemann y H. Tiziani, “Optical particle trapping with computer-generated holograms written on a liquid-crystal display”, *Optical Letters* **24**, 608–610 (1999),

[Roux04] F. S. Roux, “Distribution of angular momentum and vortex morphology in optical beams”, *Optical Communications* **242,** 45-55 (2004).

[Saavedra03] G. Saavedra, W. D. Furlan, y J. A. Monsoriu, “Fractal zone plates”, *Optical Letters* **28**, 971–973 (2003).

[Sah95] Y. Sah y G. Ranganath, “Optical diffraction in some Fibonacci structures”. *Optics Communications* **114**, 18–24 (1995).

[Spektor08] B. Spektor, A. Normatov y J. Shamir, “Singular beam microscopy”, *Applied Optics* **47**, A78 (2008)

[Swartzlander08] G. A. Swartzlander Jr, E. L. Ford, R. S. Abdul-Malik, L. M. Close y M. A. Peters, “Astronomical demonstration of an optical vortex coronagraph”, *Optical Express* **16**. 10200–10207 (2008).

[Tao06] S. H. Tao, X. C. Yuan, J. Lin y R. Burge, “Sequence of focused optical vortices generated by a spiral fractal zone plates”, *Applied Physics Letters* **89**, 031105 (2006).

[Tsao14] C. W. Tsao, Y. H. Cheng y W. J. Hsueh, “Localized modes in one-dimensional symmetric Thue-Morse quasicrystals”, *Optics Express* **22**, 24378–24383 (2014).

[Turitsyn07] S. K. Turitsyn, V. K. Mezentsev, M. Dubov, A. M. Rubenchik y M. P. Fedoruk, “Sub-critical regime of femtosecond inscription”, *Optical Express* **15,** 14750 (2007).

[Vyas07] S. Vyas y P. Senthikumaran, “Interferometric optical vortex array generator”, *Applied Optics* **46**, 2893–2898 (2007).

[Yang14] Y. Yang, W. Wang, P. Moitra, I. Kravchenko, D. Briggs y J. Valentine, “Dielectric meta reflect array for broadby linear polarization conversion y optical vortex generation”, *Nano Letters* **14**, 1394–1399 (2014).

[Zhou12] Y. Zhou, K. Panetta, S. Agaian y C. P. Chen, “Image encryption using P-Fibonacci transform y decomposition”, *Optics Communications* **285**, 594-608 (2012).

2.2 Diffractive m-bonacci lenses

Abstract

Fibonacci zone plates are proving to be promising candidates in image forming devices. In this letter we show that the set of Fibonacci zone plates are a particular member of a new family of diffractive lenses which can be designed on the basis of a given m-bonacci sequence. These lenses produce twin axial foci whose separation depends on the m-golden mean. Therefore, with this generalization, bifocal systems can be freely designed under the requirement at particular focal planes. Experimental results support our proposal.

Introduction.

Photonics technology has benefited in recent years by the emergence of several novel devices designed and constructed using quasi-periodic and fractal structures. Diffractive Optical Elements (DOEs) designed with such structures have been demonstrated unique features with multiple applications [Saavedra03, Monsoriu06, Zhang12, Furlan07, Ferrando15, Giménez10, Monsoriu04, Dai08, Verma14a, Giménez06, Ferrando13, Tao13, Calabuig13, Pu15, Cheng16, Ge12, Furlan16, Barrera12, Tebaldi09, Yadav15]. Fractal zone plates (FZPs), introduced in 2003 by our group [Saavedra03], are multifocal lenses that exhibit a wide depth of focus [Monsoriu06, Zhang12] and have low chromatic aberration [Furlan07, Ferrando15, Giménez10]. It has been shown, that the focal length of a FZP can by finely tuned by means of the so-called lacunarity of the structure [Monsoriu04, Dai08]. This feature in conjunction with

the intrinsic self-similarity of the fractal beam produce, allow simultaneous optical trapping and manipulation of multiple particles, separately, at different focal planes [Tao13, Calabuig13]. Therefore, FZP beams would be useful for constructing versatile 3D optical tweezers [Pu15, Cheng16]. FZPs have found applications in ranges of the electromagnetic spectrum outside of the visible. In a transmission X-ray microscope, FZP was proposed not only as an image-forming lens but also as a condenser element to achieve an extended depth of field [Ge12]. Promising applications in THz technology were also recently proposed [Furlan16].

FZPs are also able to perform multiplexing of encrypted data [Barrera12, Tebaldi09] and their generalized blaze counterparts: the Devil's vortex lenses provide rich phase masks which contribute to enhance security (robustness against occlusion and noise attacks) in watermarking schemes in addition to overcoming the problem of axis alignment in the optical setup [Yadav15]. Among aperiodic based DOEs, Fibonacci gratings [Verma14a, Verma14b] have been used to transform evanescent waves into propagating waves for super resolution imaging. In addition, the self similarity of these structures is important because render them robust against manufacturing defects and damages. It has been proved that DOEs with nearly 50% of degradation, can still be used in image-forming devices without loss of performance capabilities, allowing applications in harmful working conditions [Wu16]. Fibonacci zone plates [Ferrando14, Gao11, Monsoriu13, Calatayud13, Ke15] stand out for producing two foci, that are located one in front and one behind the focus of an equivalent Fresnel zone plate of the same number of zones. The axial positions of these foci are given by the Fibonacci numbers, being the golden mean the ratio of the two focal distances. The golden mean also accounts for the energetic balance of both foci and for their axial and transverse resolution.

It is important to note that the above-mentioned aperiodic based DOEs do not have special requirements to be produced (i.e. not different from the equivalent Fresnel zone plates). Indeed, several methods have been employed to do that, like printing on graphic films using a high resolution photo-plotter [Ferrando15], chemically amplified photoresist by UV laser direct writing technique [Zhang12], 3-D printing [Furlan16], and more frequently, using liquid crystal on silicon spatiallight modulators (SLMs) [Ferrando15, Dai08, Calabuig13, Pu15, Cheng16, Furlan16].

In this work, we present the m-bonacci zone plates as a meaningful generalization of the Fibonacci zone plates. The focusing properties of this family of DOEs is investigated and the imaging properties are experimentally verified.

Lens design

The new family of aperiodic diffractive lenses that we propose is inspired in the most general mathematical set of the recognized Fibonacci numbers which are known as the m-bonacci numbers [Noe, Monsoriu15].

These sets of elements $\{N_{m,j}\}$ are defined by m digits $N_{m,0}=0$, $N_{m,1}=1$ and $N_{m,j}=\sum_{i=1}^{j} N_{m,j-1}$ with $1<j<m$, and are obtained by the iterative rule $N_{m,S}=\sum_{i=1}^{m} N_{m,S-1}$ with $S\geq m$. For example, to obtain the Tribonacci numbers $(m=3)$, we define the seeds: $N_{3,0}=0$, $N_{3,1}=1$ and $N_{3,2}=1$.

The following Tribonacci numbers for $S\geq 3$ are obtained as the sum of the preceding three ones, resulting in the sequence $N_{3,i}=\{0,1,1,2,4,7,13,24,44,81\ldots\}$.

In the same way, the generalized golden mean or golden ratio is defined as the limit of the ratio of two consecutive *m*-bonacci numbers:

$$\varphi_m = \lim_{S \to \infty} \left(\frac{N_{m,S}}{N_{m,S-1}} \right). \tag{1}$$

It is easy to demonstrate that the above limit results in the transcendental equation

$$(\varphi_m)^m - \sum_{i=1}^{m} (\varphi_m)^{m-i} = 0. \tag{2}$$

The above equation for $m=2$ (Fibonacci) has the following solution $\varphi_2 \simeq 1.618$, i.e, the well-known golden ratio. For $m=3$ (Tribonacci) and $m=4$ (Tetranacci), the corresponding *m*-golden ratio are $\varphi_3 \simeq 1.839$ and $\varphi_4 \simeq 1.927$, respectively.

Based on the *m*-bonacci numbers, a binary *m*-bonacci sequence can also be generated with m binary elements, $t_{m,0} = \{0\}$, $t_{m,1} = \{1\}$, and $t_{m,j} = \{t_{m,j-1} t_{m,j-2} \ldots t_{m,0}\}$ with $1 < j < m$, and the successive elements of the sequence are obtained as the concatenation of the m previous ones, $t_{m,S} = \{t_{m,S-1} t_{m,S-2} \ldots t_{m,S-m}\}$ with $S \geq m$ [Noe]. For example, for the construction of the Tribonacci sequence $(m=3)$, we use the seeds $t_{3,0} = \{0\}$, $t_{3,1} = \{1\}$ and $t_{3,2} = \{1,0\}$. The corresponding successive elements are obtained as the concatenation rule $t_{3,S} = \{t_{3,S-1}, t_{3,S-2}, t_{3,S-3}\}$, thus $t_{3,3} = \{1010\}$, $t_{3,4} = \{1010101\}$, $t_{3,5} = \{1010101101010\}$, and so on. Therefore, the *m*-bonacci binary sequence developed up to an arbitrary level S, contains $N_{m,S}$ type-1 elements and $\sum_{i=1}^{m-1} N_{m,S-i} = N_{m,S+1} - N_{m,S}$ type-0 elements, being the limit of the ratio between both type of elements

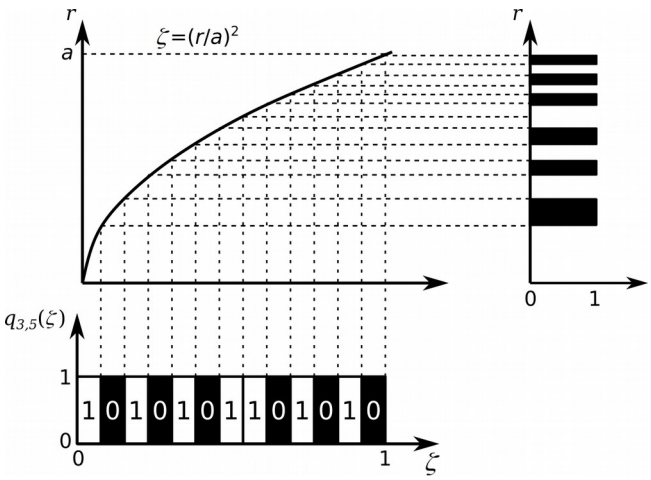

Fig. 2.10. Scheme for the construction of the radial profile of a tribonacci zone plate from the sequence $t_{3,5}=\left|1010101101010\right|$.

$$\tau_m=\lim_{S\to\infty}\left\{\frac{N_{m,S}}{N_{m,S+1}-N_{m,S}}\right\}=\frac{1}{\varphi_m-1} \tag{3}$$

Note, that the Fibonacci sequence, $\tau_2=1/\left(\varphi_2-1\right)=\varphi_2\simeq 1.618$. For the Tribonacci and Tetranacci sequences, $\tau_3=1/\left(\varphi_3-1\right)\simeq 1.191$ and $\tau_4=1/\left(\varphi_4-1\right)\simeq 1.078$, respectively.

In this work, our aim is to show how each of these sequences, developed up to a given value of S, can be used to design a zone plate (ZP). For example, as shown in Fig. 2.10, from the Tribonacci sequence, we define the binary generating function $q_{3,5}(\zeta)$ with compact support on the interval [0, 1]. Since, like a conventional Fresnel ZP, a m-bonacci ZP consists of a set of radially symmetric rings of the same area, the binary radial profile of the lens, *r*, can be obtained by performing the change of coordinates $\zeta=(r/a)^2$ where a is the external radius of the lens. The

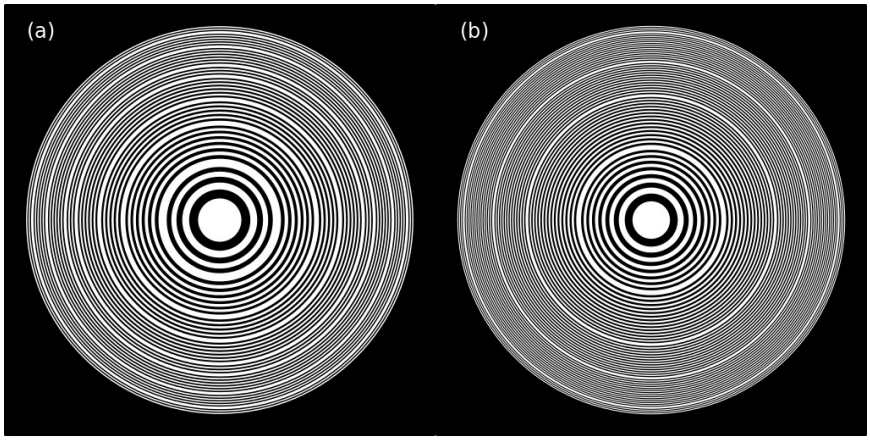

Fig. 2.11. a) Diffractive Tribonacci, m = 3, and b) Tetranacci, m = 4, lenses designed for S = 8 . The number of zones in (a) and (b) are $N_{3,8}$ = 81 and $N_{4,8}$ = 108, respectively.

transmittance of the *l*-th ring is given by the value of the *l*-th element (1 or 0) of the m-bonacci sequence $t_{m,S}$.

In this work, we propose that each of these sequences, developed up to a given value of S, can be used to design a zone plate (ZP). Like a conventional Fresnel ZP, a *m*-bonacci ZP consists of a set of radially symmetric rings of the same area, but in this case, the transmittance of the *l*-th ring is given by the value of the *l*-th element (1 or 0) of the *m*-bonacci sequence $t_{m,S,l}$. In mathematical terms, the transmittance function, $q_{m,S}$, of a *m*-bonacci ZP of order S is given by

$$q_{m,S}(\zeta)=\sum_{l=1}^{N_{m,S+1}} t_{m,S,l}\,rect(\zeta-l+1/2) \qquad (3)$$

where $\zeta=(r/a)^2$, r is the radial coordinate of the lens, and a is its maximum value. Two examples of *m*-bonacci ZPs are shown in Fig. 2.10.

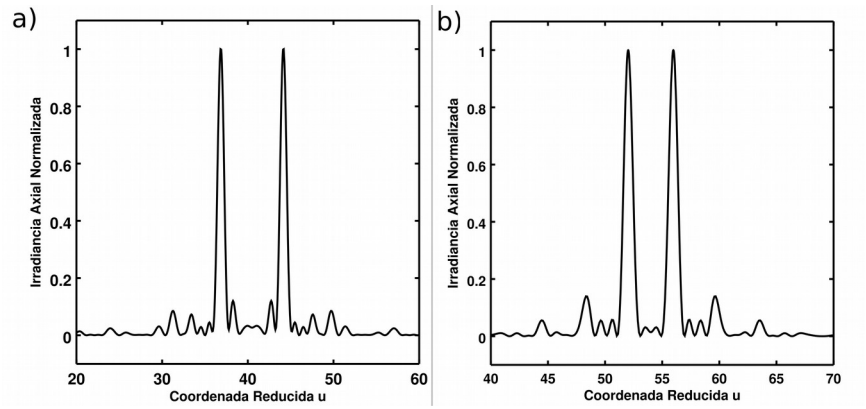

Fig. 2.12. Normalized axial irradiance versus the normalized reduced axial coordinate produced by the (a) diffractive Tribonacci and (b) Tetranacci lenses shown in Fig. 2.11.

Focusing properties.

To evaluate the focusing properties of these new diffractive lenses we have computed the axial irradiance provided by them under monochromatic plane wave illumination of wavelength λ. Within the Fresnel approximation, the irradiance along the reduced axial coordinate $u = a^2/2\lambda z$ is given by

$$\mathcal{I}(u) = 4\pi^2 u^2 \left| \int_0^1 q(\zeta) \exp(-i 2\pi u \zeta) d\zeta \right|^2 \qquad (4)$$

Two particular examples of m-bonacci lenses have been considered, both for the same level $S = 8$, the tri-bonacci and tetra-nacci zone plates: These lenses are shown in Fig. 2.11. By replacing corresponding the transmittance functions $q_{3,8}(\zeta)$ and $q_{4,8}(\zeta)$ in Eq. (5), we have numerically obtained the results shown in Fig. 2.12. It can be seen that the quasi-periodic distribution of zones according to the *m*-bonacci sequence produces a splitting of the focus (first diffraction order) in two irradiance peaks located at $u_a \simeq N_{3,8} = 44$ and $u_b \simeq N_{3,9} - N_{3,8} = 81 - 44 = 37$, for the Tribonacci

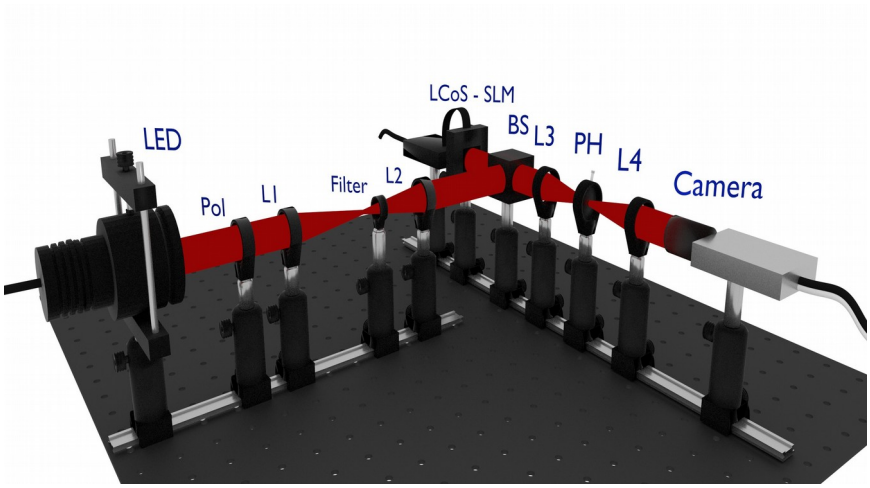

Fig. 2.13. Experimental setup. L1 and L4 are 100 mm focal distance lenses. L2 and L3 are 200 mm focal distance lenses. BS is a beam splitter, D is an iris diaphragm, and PL a linear polarizer. The translation stage shifts the camera in order to get images along z-axis (see the main text for details).

ZP; and at $u_a \simeq N_{4,8}=56$ and $u_b \simeq N_{4,9}-N_{4,8}=108-56=52$, for the Tetranacci ZP. Thus, interestingly, the ratio of the transverse distances for both lenses satisfies $u_a/u_b \simeq \tau_m=1/(\varphi_m-1)$. In fact, we have verified that, this result holds in general for every *m*-bonacci ZP. Moreover, we have also verified that this property is satisfied by *m*-bonacci ZP where the transparent and opaque zones have different area. In all these cases, the position of the two foci also tends to $u_a \simeq N_{m,S}$ and $u_b \simeq N_{m,S+1}-N_{m,S}$, but its relative maxima depend on the zones width.

Imaging properties.

To test the image forming capabilities of *m*-bonacci ZPs we have employed the experimental setup shown in Fig. 2.13. The *m*-bonacci ZPs shown in Fig. 2.11 were implemented on a Liquid Crystal in a Silicon SLM (Holoeye PLUTO, 8-bit gray-level, pixel

size 8 μm, and resolution 1920×1080 pixels), operating in amplitude mode, calibrated for 632.8 nm wavelength. The illumination system consisted of a collimated LED (Mounted High-Power LED, CW, 1000 mA). A filter allows us to select a wavelength in the visible range λ=633 nm with a bandwidth of 10 nm. The beam was collimated by the lens L1 (focal length 100 mm) and directed to a test object (a smiley face) was located at the focal plane of the achromatic Badal lens, L2 (focal length 200 mm). In addition to each *m*-bonacci lens, a linear phase carrier was modulated on the SLM to drive the light diffracted by of the odd zones of the lens out of the optical axis, generating in this way the dark zones of the amplitude lens and to avoid noise originating from the specular reflection (zero order of diffraction). This linear phase is compensated by tilting the SLM. In this way, the addressed signal was guided by the first diffraction order into the focal plane of lens L3 where a diaphragm (D) filters all diffraction orders except the first one.

Lenses L3 (focal length 200 mm) and L4 (focal length 100 mm) conform a 4f setup with 0.5 magnification. Then at the L4 lens focal plane (exit pupil) a rescaled image of the desired lens pupil is achieved. Images of the test object produced by the diffractive lenses were captured and registered with a CCD camera (8 bit gray-level, pixel pitch of 3.75 μm, and 1280 × 960 pixels) mounted on a translation stage (Thorlabs LTS 300; range 300 mm; precision 5 μm) along the optical axis (*z*).

The registered images obtained at each focal plane of a Tribonacci lens with $a=1.8$ mm and a Tetranacci lens with $a=2.078$ mm are shown in Fig. 2.14. The experimental results were reproduced without any post-processing. Note that the ratios between the image plane distances agree with the relationship $u_a/u_b=z_b/z_a\simeq\tau_m$. In fact, distances in Fig. 2.14(a) (Tribonacci) are $z_a=58$ mm and $z_b=69$ mm, and their ratio: $z_b/z_a=1.189$,

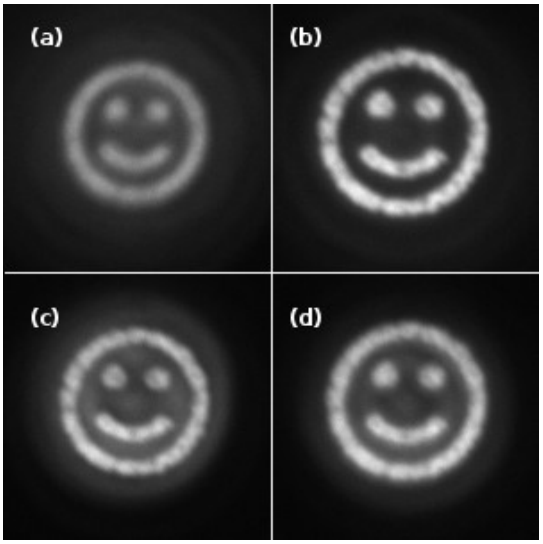

Fig. 2.14. Twin images obtained with the m-bonacci lenses shown in Fig. 2.11.

which is in good agreement with the theoretical value $\tau_3 \simeq 1.191$. (See Fig. 2.12) For the Tetranacci case, we obtained $z_c = 61$ mm and $z_d = 65$ mm and $z_d / z_c = 1.066$.

Again, this result is well matched by the predicted value $\tau_4 \simeq 1.078$. On the other hand, it can be observed that relative diameter Ø of the images at both focal planes are also related by the *m*-golden ratio. In fact, if we divide for each lens the diameter of the images shown in Fig. 2.14, we obtain approximately τ_m.

In Fig. 2.14 the resolution of the lenses is limited by the width of the outermost ring (as happens for a Fresnel zone plate). Therefore, the tribonacci lens has a lower resolution than the Tetranacci lens. On the other hand, as there are two axial foci, the images corresponding to each focus have a reduced contrast because the twin out-of-focus image is superimposed to the in-focus image. This effect is more evident when both images become

closer as happens for the Tetranacci images compared with Tribonacci ones.

Conclusions

We have presented a new family of diffractive lenses based on the generalized m-bonacci sequence. These lenses are naturally bifocals and the ratio of the two focal distances is related with the m-golden mean involved in the quasi-periodic structure. The imaging capabilities of the Tribonacci and Tetranacci lenses have been demonstrated experimentally. As the axial separation between the two foci can be tuned by a proper selection of the *m*-order, and taking into account that at present there are electronic devices that can be switchable at near real time to allow different configurations, these lenses offer a versatile alternative that can be advantageously used in several potential applications as for instance, bifocal contact and intraocular lenses, multiple plane optical trapping, optical micromachining, and confocal microscopy. Additionally, the concept of *m*-bonacci lenses can be easily extended to other geometries, like compound zone plates [Giménez10], photon sieves [Giménez06] and square zone plates [Ferrando13].

Funding

This work was supported by the Ministerio de Economía y Competitividad and FEDER (DPI2015-71256-R) and by the Generalitat Valenciana (PROMETEOII-2014-072), Spain.

Acknowledgment

F. Machado also acknowledges a fellowship of MayaNet - Erasmus Mundus, Partnership 552061-EM-1-2014-1-IT-ERA MUNDUS-EMA21 (14-0872/001-001).

References

[Barrera12] J. F. Barrera, M. Tebaldi, D. Amaya, W. D. Furlan, J. A. Monsoriu, N. Bolognini, y R. Torroba, “Multiplexing of encrypted data using fractal masks", *Optical Letters* **37**, 2895–2897 (2012).

[Calabuig13] A. Calabuig, S. Sánchez-Ruiz, L. Martínez-León, E. Tajahuerce, M. Fernández-Alonso, W. D. Furlan, J. A Monsoriu, y A. Pons-Martí, “Generation of programmable 3D optical vortex structures through devil’s vortex-lens arrays", *Applied Optics* **52**, 5822–5829 (2013).

[Calatayud13a] A. Calatayud, V. Ferrando, L. Remón, W. D. Furlan, y J. A. Monsoriu, “Twin axial vortices generated by Fibonacci lenses", *Optics Express* **21**, 10234–10239 (2013).

[Cheng16] S. Cheng, X. Zhang, W. Ma, y S. Tao, “Fractal zone plate beam based optical tweezers", *Scientific Reports* **6**, 34492 (2016).

[Dai08] H. Dai, J. Liu, S. Xuecheng, y Y. Dejin, “Programmable fractal zone plates (FraZPs) with foci finely tuned", *Optics Communications* **281**, 5515–5519 (2008)

[Ferrando13] V. Ferrando, A. Calatayud, F. Giménez, W. D. Furlan, y J. A. Monsoriu, “Cantor dust zone plates", Optics Express **21**, 2701–2706 (2013).

[Ferrando14a] V. Ferrando, A. Calatayud, P. Andrés, R. Torroba, W. D. Furlan, y J. A. Monsoriu, “Imaging properties of Kinoform Fibonacci lenses", *IEEE Photonics Journal*. **6**, 6500106 (2014).

[Ferrando15] V. Ferrando, F. Giménez, W. D. Furlan, y J. A. Monsoriu, “Bifractal focusing y imaging properties of Thue-Morse Zone Plates", *Optics Express* 23, 19846–19853 (2015)

[Furlan07] W. D. Furlan, G. Saavedra, y J. A. Monsoriu, “White-light imaging with fractal zone plates", *Optical Letters* **32**, 2109–2111 (2007)

[Furlan16a] W. D. Furlan, V. Ferrando, J. A. Monsoriu, P. Zagrajek, E. Czerwińska, y M. Szustakowski, “3D printeddiffractive terahertz lenses", *Optical Letters* **41**, 1748–1751 (2016).

[Gao11] N. Gao, Y. Zhang, y C. Xie, “Circular Fibonacci gratings", *Applied Optics* **50**, G142–G148 (2011).

[Ge12] X. Ge, Z. Wang, K. Gao, D. Wang, Z. Wu, J. Chen, Z. Pan, K. Zhang, Y. Hong, P. Zhu, y Z. Wu, “Use offractal zone plates for transmission X-ray microscopy", *Analytical y Bioanalytical Chemistry* **404**, 1303–1309 (2012).

[Giménez06] F. Giménez, J. A. Monsoriu, W. D. Furlan, y A. Pons, “Fractal photon sieve", *Optics Express* **14**, 11958–11963 (2006)

[Giménez10] F. Giménez, W. D. Furlan, A. Calatayud, y J. A. Monsoriu, “Multifractal zone plates", *Journal of the Optical Society of America A* **27**, 1851–1855 (2010)

[Ke15] J. Ke y J. Zhang, “Generalized Fibonacci photon sieves", *Applied Optics* **54**, 7278–7283 (2015).

[Monsoriu04] J. Monsoriu, G. Saavedra, y W. Furlan, “Fractal zone plates with variable lacunarity", *Optics Express* **12**, 4227–4234 (2004)

[Monsoriu06] J. A. Monsoriu, C. J. Zapata-Rodriguez y W. D. Furlan, “Fractal axicons", *Optics Communications* **263**, 1–5 (2006)

[Monsoriu13] J. A. Monsoriu, A. Calatayud, L. Remón, W. D. Furlan, G. Saavedra, y P. Andrés, “Bifocal Fibonacci diffraction lenses", *IEEE Photonics Journal* **5**, 3400106 (2013).

[Monsoriu15] J. A. Monsoriu, M. H. Giménez, W. D. Furlan, J. C. Barreiro, y G. Saavedra, “Diffraction by m-bonacci gratings", *European Journal of Physics* **36**, 65005 (2015).

[Noe] T. Noe, T. Piezas, y E. W. Weisstein, “Fibonacci n-Step Number", From MathWorld–A Wolfram WebResource. http://mathworld.wolfram.com/Fibonaccin-StepNumber

[Pu15] J. Pu y P. H. Jones, “Devil’s lens optical tweezers", *Optics Express* **23**, 8190–8199 (2015).

[Saavedra03] G. Saavedra, W. D. Furlan, y J. A. Monsoriu, “Fractal zone plates”, *Optical Letters* **28**, 971–973 (2003).

[Tao13] S. H. Tao, B. C. Yang, H. Xia, y W. X. Yu, “Tailorable three-dimensional distribution of laser foci based oncustomized fractal zone plates", *Laser Physics Letters* **10**, 035003 (2013).

[Tebaldi09] M. Tebaldi, W. D. Furlan, R. Torroba, y N. Bolognini, “Optical-data storage-readout technique based onfractal encrypting masks", *Optical Letters* **34**, 316–318 (2009).

[Verma14a] R. Verma, M. K. Sharma, P. Senthilkumaran, y V. Banerjee, “Analysis of Fibonacci gratings y theirdiffraction patterns", *Journal of the Optical Society of America A* **31**, 1473–1480 (2014)

[Verma14b] R. Verma, V. Banerjee, y P. Senthilkumaran, “Fractal signatures in the aperiodic Fibonacci grating", *Optical Letters* **39**, 2557–2560 (2014).

[Wu16] K. Wu y G. P. Wang, “Two-dimensional Fibonacci grating for far-field super-resolution imaging", *Scientific Reports* **6**, 38651 (2016).

[Yadav15] A. K. Yadav, S. Vashisth, H. Singh, y K. Singh, “A phase-image watermarking scheme in gyrator domainusing devil’s vortex Fresnel lens as a phase mask", *Optics Communications* **344**, 172–180 (2015).

[Zhang12] Q. Zhang, J. Wang, M. Wang, J. Bu, S. Zhu, B. Z. Gao, y X. Yuan, “Depth of focus enhancement of amodified imaging quasi-fractal zone plate", *Optics & Laser Technology* **44**, 2140–2144 (2012)

2.3 Multi-image formation by Walsh zone plates

Abstract

In this paper we report the achievement of the first multi-images to our knowledge obtained with radial Walsh filters working as aperiodic diffractive lenses. Derived from Walsh functions, radial Walsh filters are phase binary diffractive optical elements characterized by a set of equal-area concentric rings that take the phase values 0 or π, corresponding to transmittance values +1 or -1 of the corresponding Walsh function. Then, a radial Walsh filter can be re-interpreted as an aperiodic zone plate with self-similar multi-focusing properties under monochromatic plane wave illumination and, therefore, multi-imaging capabilities.

Introduction

The Walsh functions were introduced into mathematics as of a set piecewise constant functions satisfying orthogonality conditions over the unit interval [Walsh23]. The functions take values +1 and -1 on sub-intervals defined by dyadic fractions, being the number of zero crossings determined by the order of the Walsh function. These functions are of great practical interest in many field, especially in communications [Harmuth69] or digital signal processing [Harmuth69].

Derived from Walsh functions in polar coordinates, radial Walsh filters with rotational symmetry have been implemented for tackling problems of optical image formation [Hazra77]. For example, these filters have been proved to be useful in the treatment of apodization problems [Hazra76] or for tailoring of

resolution in microscopic applications [Hazra07]. Earlier studies on radial Walsh filters have shown that the corresponding axial and transverse intensity distributions in the far-field diffraction patterns present self-similar properties [Mukherjee14a, Mukherjee14b].

On the other hand, as is its well-known, a conventional Fresnel zone plate consists of alternating transparent-opaque circular rings (or alternating 0 and π phase shift ring zones) and whose radii are proportional to the square root of the natural numbers [Ojeda-Castañeda96]. Thus, the transmittance of the lens can be generated from a one-dimensional compact-supported periodic function $q(\varsigma)$, followed by a change of coordinates $\varsigma = (r/a)^2$, where r is the radial coordinate and a the radius of the lens. Fresnel zone plates are essential diffractive lenses for focusing and imaging in many scientific and technological areas, as for example in THz [Wang13] or X-Ray [Mohacsi17] applications.

In order to improve the behavior of conventional zone plate, fractal zone plates [Saavedra03, Davis04] where introduced in the literature as a novel aperiodic diffractive lenses with self-similar focusing properties [Monsoriu04] and extended depth of field imaging [Furlan07]. Fractal zone plates are characterized by its fractal structure along the squared radial coordinate ς. Other interesting mathematical generators, $q(\varsigma)$, of aperiodic zone plates are the Fibonacci and Thue-Morse sequences [Maciá06]. Fibonacci zone plates are intrinsically bifocals, being the ratio of the two main focal distances defined by the golden ratio [Monsoriu13]. Thue-Morse zone plates combine the properties of fractal and Fibonacci zone plates producing two main self-similar foci along the optical axis with extended depth of focus [Ferrando15].

In this work, radial Walsh filters are re-interpreted as aperiodic zone plates by replacing the periodic function $q(\varsigma)$, by a given Walsh function. To evaluate the focusing and imaging

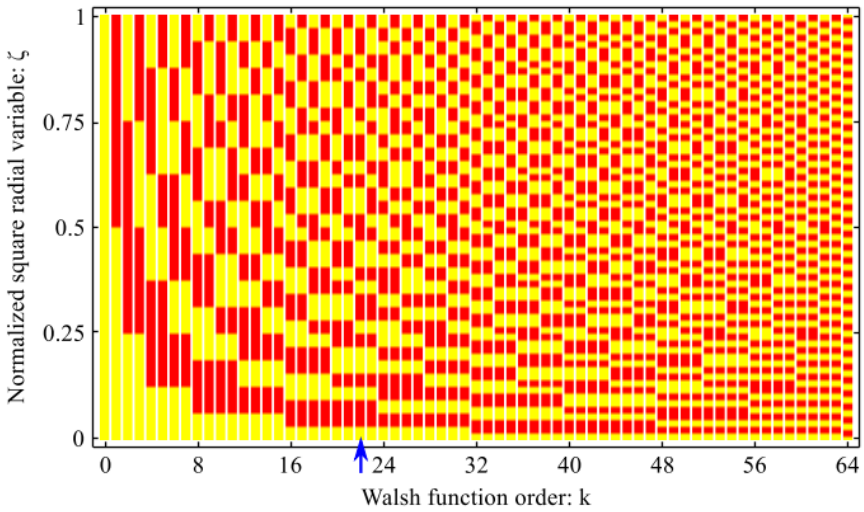

Fig. 2.15. Graphical representation of the Walsh functions up to order k = 64. The yellow barscorrespond to the value +1 while the red bars correspond to the value −1. The blue arrow indicates the order k = 22, which has been used to design the WZP shown in Fig. 2.

properties of the WZPs we have implemented these diffractive lenses with a spatial light modulator in an image forming experiment. It is shown that WZPs produces multiple foci along the optical axis, so as an image-forming devices, WZPs present unconventional optical multi-imaging capabilities. Using aperiodic Walsh functions, we have design new quadrifocal diffractive lenses improving in this way the response of previous aperiodic zone plates.

Focusing properties

Let us start revisiting the original proposal for the radial Walsh filters [Hazra77]. It was based on the Walsh functions represented in Fig. 2.15. The first step in the construction procedure consist of representing the binary decomposition of an integer number *k* in the form

$$bin\, k = \sum_{i=0}^{m-1} (k_b)_i 2^i, \tag{1}$$

where $(k_b)_i$ is the i-th bit, 0 or 1, of the binary numeral for k and m is the lowest integer number for which $2^m > k$, i.e., 2^m is the power of 2 that exceeds k, and $(k_b)_0$ is the LSB. Based on this decomposition, the corresponding Walsh function of order k, $q_k(\varsigma)$, can be defined in the interval $\varsigma \in [0,1]$ as

$$q_k(\zeta) = \prod_{i=0}^{m-1} sgn[\cos(\pi 2^i k_i \zeta)] \tag{2}$$

The function $\mathrm{sgn}[x]$ is defined as

$$sgn[x] = \begin{cases} +1, & x>0 \\ 0, & x=0 \\ -1, & x<0 \end{cases} \tag{3}$$

In Fig. 2.15 we have represented the Walsh functions, $q_k(\varsigma)$, up to order $k = 64$. The yellow bars correspond to the value +1 while the red bars correspond to the value −1. Note that the number of zero crossings is determined by the order of the Walsh function k.

From a particular Walsh function, $q_k(\varsigma)$, the corresponding radial Walsh filter can be generated by performing a change of variable $\varsigma = (r/a)^2$ and by rotating the transformed Walsh function around ones of its extremes. The result is a pure phase DOE having a radial coordinate r and radius a. In this way, we can re-interpret a radial Walsh filter of order k as a binary phase aperiodic zone plate whose transmittance is defined by the Walsh function, $q_k(\varsigma)$, expressed in the normalized squared radial coordinate ς.

Figure 2.16a shows a WZP of order $k = 22$ characterized by a set of concentric zones that take the phase values 0 (yellow rings)

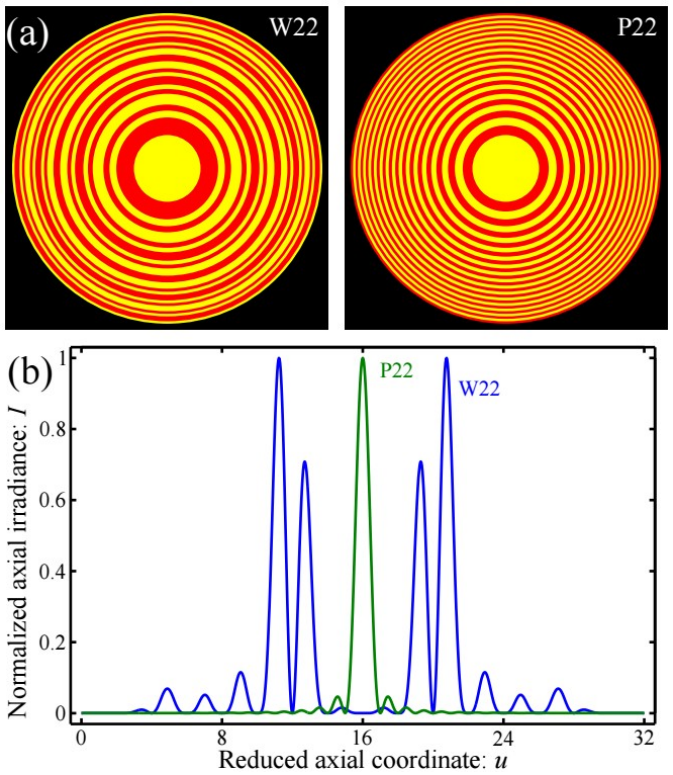

Fig. 2.16. (a) WZP generated from the 1-D function q 22 (ς) shown in Fig 2.15 and its equivalentFresnel zone plate of the same resolution. Yellow and red rings correspond to a phase 0 (+1transmittance value) and π (−1 transmittance value), respectively. (b) Numerically computed axial irradiance produced by both lenses shown against the reduced axial coordinate u.

or π (red rings), corresponding to transmittance values +1 or −1, respectively.

For comparison, a conventional phase binary zone plate with the same resolution (same width of the outermost zone) is also represented in the same figure. Note that the equivalent Fresnel zone plate can be obtained using the same procedure but by

replacing the aperiodic Walsh function with a periodic one, i.e., a sequence of alternating zones in opposite phase. In other words, a WZP can be understood as a binary phase zone plate where the positions of some phase zones has been interchanged.

To evaluate the focusing properties of the WZPs, we have computed the axial irradiances provided by these aperiodic lenses under monochromatic plane-wave illumination. Within the Fresnel approximation, the axial irradiance function is given by

$$(u) = 4\pi^2 u^2 \left| \int_0^1 q(\zeta) \exp(-i 2\pi u \zeta) d\zeta \right|^2 \qquad (4)$$

where $u = a^2/2\lambda z$ is the reduced axial coordinate, z is the axial distance from the pupil plane, and λ is the wavelength of the light. Thus, the axial irradiance can be defined in terms of the Fourier transform of the mapped pupil function $q(\varsigma)$. By using Eq. (4) we have computed the axial irradiance (corresponding to the first-order diffraction foci) provided by a WZP of order $k = 22$ and its equivalent periodic zone plate. The result shown in Fig. 2.16(b) proves that the reordering of the phase zones according to the aperiodic Walsh function produces a multiple splitting of the first-order focus generating, in our case, four foci along the axial coordinate. Therefore, Walsh functions can be implemented in the design of novel multifocal diffractive lenses with multi-imaging capabilities. Due to the binary nature of the diffraction structure, high diffraction orders also appear (not shown in Fig. 2.16), so these four foci are replicated along the reduced axial coordinate u with a period corresponding to the number of zones, N.

We have also computed in Fig. 2.17 the axial irradiance of WZPs for different orders, k. For comparison, the normalized reduced axial coordinate, $u' = u/N$, has been considered, focusing our attention around the first diffraction order. The gray-code bars give the normalized axial irradiance, I, of theses diffractive

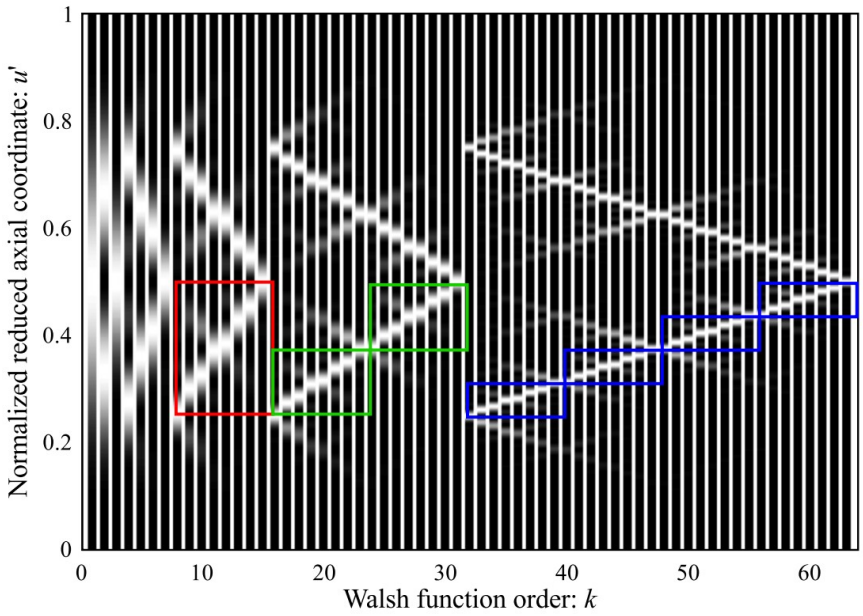

Fig. 2.17. The grey-code bars represent the normalized axial irradiances, I, for WZPs of differentorders k, being I = 1 in the white regions and I = 0 in the black regions. The reduced axialcoordinate has been normalized to u´ = u/N, where N is the number of zones. The red, greenand blue boxes show the same structure at different scales.

aperiodic lenses, being $I = 1$ in the white regions and $I = 0$ in the black regions.

First, we can easily identify the four foci shown in Fig. 2.16(b) in the irradiance bar in Fig. 2.17 for k =22. Note that the four focal distances can be modulated with the parameter k. It is also shown that this quadrifocal configuration is preserved for different orders k, although more subsidiary foci appear for large k values. It can also be seen that the four foci collapse to a single focus for $k = 1, 3, 7, 15, 31, 63, \ldots = 2^n\text{-}1$ with $n = 1, 2, 3, 4\ldots$since the structure of the corresponding WZP matches with a conventional periodic zone plate.

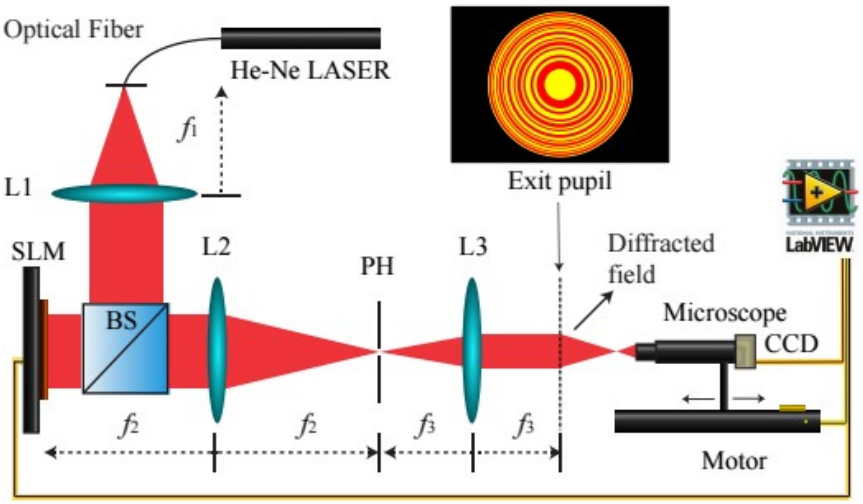

Fig. 2.18. Experimental setup for the assessment of (a) the multi-focusing properties of WZPs and(b) the multi-imaging capabilities by replacing the laser light source by a monochromatic LEDilluminating a binary object (a smiley face).

On the other hand, the irradiances produced by WZPs under monochromatic plane-wave illumination present self-similar properties. For instance, the irradiances shown in the red box for $8 \le k \le 15$ are replicated on a smaller scale in the two green boxes for $16 \le k \le 31$ and even on smaller scale in the four blue boxes for $32 \le k \le 63$. The property of self-similarity in axial intensity distributions of radial Walsh filters was also reported in the far field diffraction patterns [8]. We have extended this property to the axial irradiances provided by WZPs working as aperiodic diffractive lenses.

Imaging properties

We have experimentally tested the multi-imaging capabilities of aperiodic WZPs and compared their performance against a conventional Fresnel zone plates of the same resolution. A

schematic illustration of the experimental setup is shown in Fig. 2.18(a).

The diffractive lenses under study were implemented on a Liquid Crystal in a Silicon SLM (Holoeye PLUTO with 8-bit gray-level, a pixel pitch of 8 μm, and a resolution equal to 1920×1080 pixels). The SLM operating in phase-only modulation mode was calibrated for a 2π phase shift at λ = 633 nm. In order to avoid the noise originated from the specular reflection (zero order diffraction) and from the higher diffraction orders due to the pixelated structure of the SLM, a linear phase carrier was also modulated on the SLM in addition to the WZP phase profile.

This linear phase was compensated by tilting the SLM and by using a pin-hole (PH) to filter all diffraction orders except the first one into the focal plane of lens L2. In this way, a rescaled image of the diffractive lens was achieved at the L3 lens focal plane (exit pupil).

A collimated beam from a He-Ne laser (λ = 633 nm) was directed onto the SLM. The diffracted field was captured and registered with a microscope (4x Zeiss Plan-Apochromat objective) attached to a CCD camera (8 bit gray-level with a pixel pitch of 3.75 μm and 1280×960 pixels). The microscope and the CCD were mounted on a translation stage (Thorlabs LTS 300 with a range of 300 mm and a precision of 5 μm) along the optical axis. The experimental irradiances obtained for a WZP of order k = 22 and radius a = 1.74 mm is shown in Fig. 2.19(a).

A profile of the measured axial irradiance is represented in Fig. 2.19(b), together with the results numerically computed using Eq. (4). A very good agreement between theory and experiment can be observed and the four foci marked with the characters [A-D] are clearly visible. The corresponding focal distances were f_A=114.9 mm, f_B=124.8 mm, f_C=188.2 mm, and f_D=211.7 mm.

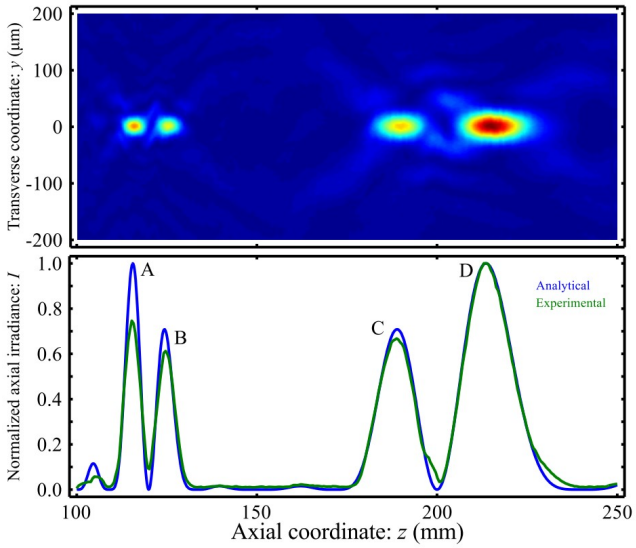

Fig. 2.19. (a) Experimental transverse intensity distribution produced by a WZP of order k = 22.(b) Profile of Fig. 5(a) (blue line) showing the axial irradiance distribution. The theoreticalvalues of the irradiance are shown in green line for comparison. In both cases, the values arenormalized to the peak intensity.

In order to verify the multi-imaging capabilities of a WZP we have modified the previous experimental setup as shown in Fig. 2.18(b). We replaced the He-Ne laser source by a binary object (a smiley face) located at the focal plane of the achromatic Badal lens, L1. The illumination system consisted of a red collimated LED (Mounted High-Power LED, red 625 nm, 1000 mA) and a bandpass filter (λ = 632.8 nm ± 0.6 nm). The multiple images produced by the aperiodic diffractive lens were captured with same image registration system (the CCD camera mounted on the translation stage).

Figure 2.20 shows the images provided by the multifocal WZP of order k = 22 and the equivalent monofocal Fresnel zone

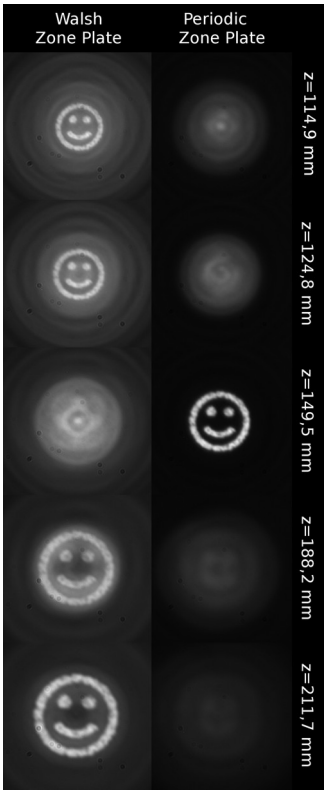

Fig. 2.20. Images obtained with the WZP of order k = 22 and with the equivalent periodic zone plate of the same resolution. Five different location, z, were considered corresponding to the four image planes of the quadrifocal WZP (first, second, fourth and fifth rows) and the image plane of the monofocal Fresnel lens (third row).

plate. The experimental results were reproduced without any post-processing.

The registered images were obtained at each focal plane that can be tuned by a proper selection of the parameter *k*. Note that the image provided by the Fresnel zone plates have higher contrast

than those provided by the WZP. This is a common problem for all multifocal lenses since the out-of-focus images are superimposed to the in-focus image.

Nevertheless, as can be seen, four clear images were captured at the focal planes [A-B] depicted in Fig. 2.19(b), demonstrating in this way the multi-imaging capabilities of the WZP as quadrifocal diffractive lens.

Summary

In this work we have demonstrated the multi-imaging capability of radial Walsh filters reinterpreted as aperiodic zone plates. First, we have shown that a WZP naturally produces multiple foci along the axial coordinate. A very good agreement between the experimental and the theoretical results has been obtained. Then, the first images produced by these kind of filters working as quadrifocal diffractive lenses are reported. As the axial separation between the foci can be tuned by a proper selection of the Walsh order, *k*, these lenses offer a versatile alternative that can be advantageously used in several potential applications as for instance, multifocal contact and intraocular lenses, multiple plane optical trapping, optical micromachining, and confocal microscopy, among others.

Acknowledgments

This study was supported by the Ministerio de Economía y Competitividad and FEDER (DPI2015-71256-R), Spain, and by the Generalitat Valenciana, (PROMETEO II-2014-072), Spain.

Federico Machado has been supported by the MayaNet - Erasmus Mundus Partnership 552061-EM-1-2014-1-IT-ERA MUNDUS-EMA21 (2014-0872/001-001).

References

[Beauchamp84] K.G. Beauchamp, *Applications of Walsh y related functions*, Academic Press, London (1984).

[Davis04] J. A. Davis, L. Ramirez, J. A. Rodrigo Martín-Romo, T. Alieva y M. L. Calvo, “Focusing properties of fractal zone plates: Experimental implementation with a liquid-crystal display", *Optics Letters* **29**, 1321–1323 (2004).

[Ferrando15] V. Ferrando, F. Giménez, W. D. Furlan y J. A. Monsoriu, “Bifractal focusing y imaging properties of Thue-Morse Zone Plates", *Optics Express* **23**, 19846–19853 (2015).

[Furlan07] W. D. Furlan, G. Saavedra y J. A. Monsoriu, “White light imaging with fractal zone plates", *Optics Letters* **32**, 2109– 2111 (2007).

[Harmuth69] H.F. Harmuth, “Applications of Walsh functions in communications", *IEEE Spectrum* **6**, 82–91 (1969).

[Hazra07] L.N. Hazra, “Walsh filters for tailoring of resolution in microscopic imaging", *Micron* **38**(2), 129–135 (2007).

[Hazra76] L.N. Hazra y A. Banerjee, “Applications of Walsh functions in generation of optimum apodizers", *Journal of Optics* **5**, 19–26 (1976).

[Hazra77] L.N. Hazra, “A new class of optimum amplitude filters", *Optics Communications* **21**, 232–236 (1977).

[Maciá06] E. Maciá, “The role of aperiodic order in science y technology", *Reports on Progress in Physics* **69**, 397–441 (2006).

[Mohacsi17] I. Mohacsi, I. Vartiainen, B. Rösner, M. Guizar-Sicairos, V.A. Guzenko, I. McNulty, R. Winarski, M.V. Holt y C. David, “Interlaced zone plate optics for hard X-ray imaging in the 10 nm range", *Scientific Reports* **7**, 43624 (2017).

[Monsoriu04] J. A. Monsoriu, G. Saavedra y W. D. Furlan, “Fractal zone plates with variable lacunarity", *Optics Express* **12**, 4227–4234 (2004).

[Monsoriu13] J. A. Monsoriu, A. Calatayud, L. Remon, W. D. Furlan, G. Saavedra y P. Andrés, “Bifocal Fibonacci diffractive lenses", *IEEE Photonics Journal* **5**, 3400106 (2013).

[Mukherjee14a] P. Mukherjee y L.N. Hazra, “Self-similarity in radial Walsh filters y axial intensity distributions in the far-field diffraction patterns", *Journal of Optical Society of America* **31**, 379–387 (2014).

[Mukherjee14b] P. Mukherjee y L.N. Hazra, “Self-similarity in transverse intensity distributions in farfield diffraction patterns of radial Walsh filters", *Advances in Optics* **2014**, 352316 (2014).

[Ojeda-Castañeda96] J. Ojeda-Castañeda y C. Gómez-Reino, *Selected Papers on Zone Plates*, SPIE Optical Engineering Press (1996).

[Saavedra03] G. Saavedra, W.D. Furlan y J.A. Monsoriu, "Fractal zone plates," *Optics Letters* **28**, 971–973 (2003).

[Walsh23] J. L. Walsh, “A closed set of normal orthogonal functions", *American Journal of Mathematics* **45**, 5–24 (1923).

[Wang13] X. Wang, Z. Xie, W. Sun, S. Feng y . Cui, J. Ye y Y. Zhang, “Focusing y imaging of a virtual all-optical tunable terahertz Fresnel zone plate", *Optics Letters* **38**, 4731–4734 (2013).

2.4 Terahertz Sieves

Abstract

Imaging at terahertz (THz) frequencies offers a great potential for applications including: security screening, telecommunications biodetection, and spectroscopy. Some of these applications need specially designed lenses with customized characteristics that are not commercially available. In this work we present the THz sieves as a new kind of THz lenses. We demonstrate that these lenses improve the resolution of conventional zone plates constructed with the same level of detail. Amplitude and phase THz sieves were 3-D printed and tested experimentally. Excellent agreement was obtained between the experimental and calculated results.

Introduction

Numerous applications of THz an sub-THz radiation such as imaging or spectroscopy require passive devices like lenses [Scherger11], filters [Wilk09], and waveguides [D'Auria15]. Focusing lenses allow improving the sensitivity of terahertz setups, which is a crucial issue in this range of electromagnetic radiation, where there is a lack of high-power sources and high-sensitive detectors.

The optical properties of different polymers [Podzorov08] have been exploited to fabricate a variety of THz lenses that are commercially available. However, many applications require custom-made THz lenses with a special design. Refractive lenses with different geometries have been manufactured from bulk polymers by lathe turning, compression molding [Scherger11], and

recently, by 3D printing [Busch14, Squires15]. On the other hand diffractive THz optical elements have been proposed and tested [Wang02, Yu09]. In spite of their lower light throughput and chromatic aberration, diffractive lenses can have high numerical aperture [Siemion12], and permit beam shaping [Furlan16, Liu16], working in linear and compact setups. Therefore, in many applications, the performance of diffractive THz lenses is better than that of their refractive homologous. Additionally, 3D printing technology has also been used recently to construct special designs of diffractive lenses [Furlan16, Liu16, Suszek15].

As different materials used for 3-D printing have low refractive index and a frequency-dependent absorbance in the THz bandwidth, several 3-D printing materials were tested previously in our previous paper [Furlan16]. In particular, using THz time-domain spectroscopy we measured the absorption coefficients and refractive index of nylon polyamide (PA6) and acrylonitrile-butadiene-styrene with different densities in the 0.1 - 2.0 THz frequency range.

Photon sieves (PSs) are diffractive optical elements, originally conceived to improve X-rays focusing [Kipp01]. The first PSs where basically amplitude Fresnel zone plates (FZPs) in which the transparent rings were substituted by non-overlapping holes of different sizes. Special features of PSs in the visible range were investigated in several works [Cao03, Giménez06, Giménez07, Sabatyan11], from which different applications emerged [Menon05, Andersen05].

The main features that characterize PSs are the following:

(1) They can be fabricated on a single sheet without any substrate,

(2) PS allow a better resolution than a Fresnel zone plate (FZP), with the same dimensions [Kipp01],

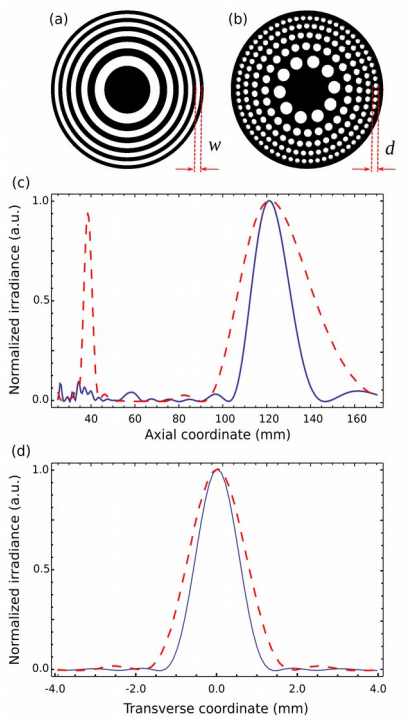

Fig. 2.21. a) Binary Fresnel zone plate, w is the width of the outermost zone, which determines its transverse resolution. b) THz sieve with the same number of Fresnel zones, d is the diameter of the holes at the Fresnel zone corresponding to w. c) Numerical axial point spread function; and d) Transverse Intensity at the focal plane, computed for a FZP (dashed line) and a TS (continuous line) of the same focal distance (f=122 mm; v0=0.625 THz). In Fig. 1c) and Fig. 1d) each plot was normalized to its maximum value.

(3) they allow improved focusing by the suppression of secondary maxima and higher orders of diffraction [Giménez07, Sabatyan11].

In this work, we introduce the THz sieves (TS). We study the TS axial and transverse resolution in comparison with those provided by a conventional FZP constructed with the same level of

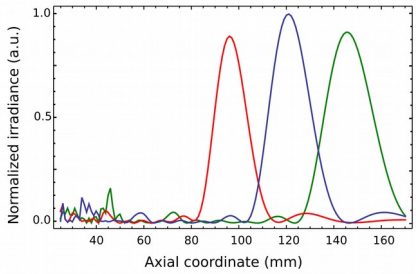

Fig. 2.22. TS performance at 3 different frequencies: v_1=0.625 THz (blue line); v_1=0.496 THz (red line) and v_2=0.741 THz (green line). The maximum value of the irradiance for the design frequency was used for normalization.

detail. The focusing properties of both, amplitude and phase TS are experimentally demonstrated.

TSs Design and focusing properties

The construction procedure of a TS starts from a conventional FZP designed for a given THz frequency. As it is well known, an amplitude FZP of focal length f at wavelength λ, consists of alternate transparent and opaque zones, where the radius of the n-th zone is given by $r_n^2 = 2nf\lambda + n^2\lambda^2$.

The width of outermost ring of a zone plate with N zones, $w = r_N - r_{N-1}$ (see Fig. 2.21a), imposes a limit on the maximum resolution achievable with the FZP: $w = 2\lambda f / 2r_N$. It was shown [Kipp01] that a PS can overcome this limitation because the pinhole diameter can be bigger than the width of the underlying zone. Thus a PS can have a higher numerical aperture than a FZP constructed with the same level of detail. This property is of particular interest in THz applications, where low-cost diffractive lenses can be 3D printed.

A TS is constructed by replacing the transparent rings of width *w* in the Fresnel zone plate by non-overlapping circular holes of diameter *d* distributed about the rings (see Fig. 2.21b). Thus, the transmittance function $t(x,y)$ of a TS can be expressed as a binary function that takes the values $t(x,y)=1$ if $(x-x_{i,j})^2+(y-y_{i,j})^2 \le d_{i,j}^2$; and either $t(x,y)=0$ or $t(x,y)=1$, otherwise; depending on if the TS is of amplitude or phase, respectively. In the transmittance function, $x_{i,j}$ and $y_{i,j}$ are the center coordinates of the *i*-th hole.

The focusing properties of our proposal were assessed in comparison with a FZP by means of the irradiance at different planes for a point object at infinity i.e.; the point spread function (PSF). This function was computed numerically by using the nonparaxial scalar diffraction theory:

$$I(x,y;z)=\frac{1}{\lambda^2}\left|\int\int t(x_0,y_0)\frac{\exp\left\{\frac{2\pi}{\lambda}\sqrt{(x-x_0)^2+(y-y_0)^2+z^2}\right\}}{\sqrt{(x-x_0)^2+(y-y_0)^2+z^2}}\right| \qquad (1)$$

We employed Eq. (1) to compare the focusing properties of phase TS and FZP. In particular we analyzed two lenses of the same focal distance: $f = 122$ mm, at the same design frequency: $\nu_0 = 0.625$ THz. For the lens material we considered polyamide PA6, which has a refractive index n=1.6 at this frequency [10]. The radius of the FZP ($r_N = 18.8$ mm), and its outermost width ($w = 1.63$ mm), were both selected to be compatible with an experimental verification in our lab. For the TS the minimum hole diameter was fixed to be d_{min}=1.65mm; i.e.; approximately of the same size of *w*.

The maximum hole diameter was $d_{max} = 4.11$ mm. The hole density in each zone was selected such as the transparent area in each TS zone must be at least a 75% of the whole Fresnel zone. With these parameters we used Eq. (1) to compute the axial irradiance provided by the TS for different values of *d*, in the range

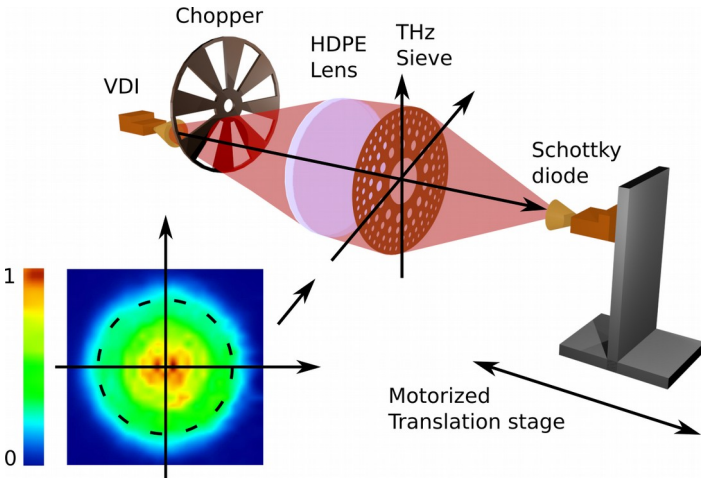

Fig. 2.23. Experimental setup used in axial PSF measurements. The source of THz is a VDI frequency multiplier with a horn antenna. The divergent beam, is collimated by a HDPE refractive lens (focal distance f =150 mm). The transverse intensity measured at TS plane (x,y) is shown in the inset. The radius of the dashed line in the inset is r_N = 18.8 mm. The detector: a Schottky diode, with a horn antenna, mounted on a 3D motorized stage, scanned the focal volume. A lock-in system, based on modulation at 187 Hz, and a mechanical chopper, was employed to measure the signal from the detector.

$1w \le d \le 2w$, obtaining that the value d = 1.33, w provided the best apodization of the third diffraction order focus. Thus, we found that with the same width of the outermost ring, the numerical aperture of the TS is 1.33 times higher than the FZP, being the TS radius r_N = 25 mm.

The axial irradiances and transverse intensities at the focal plane, provided by both lenses are shown in Figs. 2.21c and 2.21d, respectively. As can be seen in Figs. 2.21c and 2.21d both the axial and transverse resolution are better for the TS. The full width at half maximum (FWHM) of the axial irradiance peak provided by the TS is 18.8 mm, which is 52% lower than FWHM of the FZP. For the transverse resolution the FWHM at the focus of the TS is

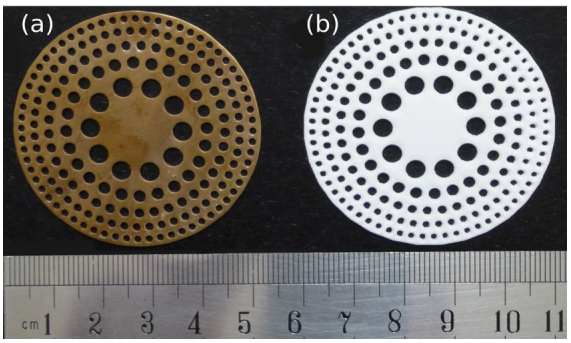

Fig. 2.24. 3D printed THz sieves. a) Is an amplitude lens made in bronze. b) Is a phase lens made in PA6 polyamide. The holes are located in the even zones of a Fresnel zone plate (focal distance f= 122 mm).

1.31 mm, and 1.77 mm for the FZP.

The apodization of the third order focus at z = 40 mm can be clearly seen in Fig. 2.21c. The physical reason for this apodization is that the axial irradiance only depends on the angular average of the effective pupil along the radial coordinate [20], which in the case of TS is smoothed by effect of the holes. On the other hand, as expected [Kipp01], we also found that the diffraction efficiency of the FZP was higher (40.5%) than the diffraction efficiency of the TS (18.4%).

In order to investigate the effect of a finite bandwidth on TS performance, we have computed the axial PSF for the TS at two other frequencies. The result is shown in Fig. 2.22. In this case in addition to the focal shift produced by the chromatic aberration of the TS, the peak intensity is lower for the other two frequencies because for these frequencies the phase difference between the holes and the plate is not exactly π.

Experimental results

Fig. 2.23 shows the setup we employed for the experimental characterization of the TSs. A VDI frequency multiplier (Virginia Diodes, Inc. Charlottesville, VA. USA) provided the 0.625 THz beam. The source of microwave radiation for the VDI frequency multiplier was an electromagnetic YIG-tuned oscillator MLXB-1768PA. It generates radiation in frequency range 13-15 GHz. The base frequency was multiplied 48 times. The divergent beam, emerging from the horn antenna, was collimated by a high density polyethylene (HDPE) lens and directed to the investigated TS. The detector: a Schottky diode, was mounted on a 3D motorized stage.

The focal spot was scanned with a horn antenna, having a 2.4 mm aperture diameter. A lock-in system, based on modulation at 187 Hz, and a mechanical chopper, was employed to measure the signal from the detector. The inset in Fig 2.23 shows the intensity recorded at the transverse plane (x,y) just before the lens plane.

Two different TS lenses were fabricated by 3D printing: an amplitude lens, shown in Fig. 2.24a, constructed in bronze, and a phase lens, shown in Fig 2.24b, made in PA 6 polyamide (refractive index 1.6 and absorption coefficient 3.09 cm^{-1} at 0.625 THz). The physical dimensions of both lenses were the same, and coincide with those used to compute Fig. 2.21c and Fig. 2.21d). As the minimum thickness of the phase TS that provides a π phase difference between the lenses material and the holes $t=\lambda/2(n-1)=0.4\,\mathrm{mm}$, was considered too thin to be handled, we have constructed the lenses with a thickness of $3t=1.2\,\mathrm{mm}$, which produces the same phase shift. Other details of the 3D lens production can be found elsewhere [Furlan16].

Fig. 2.25 shows the experimental results obtained for the axial PSF (dotted lines) corresponding to the lenses shown in Fig. 2.24.

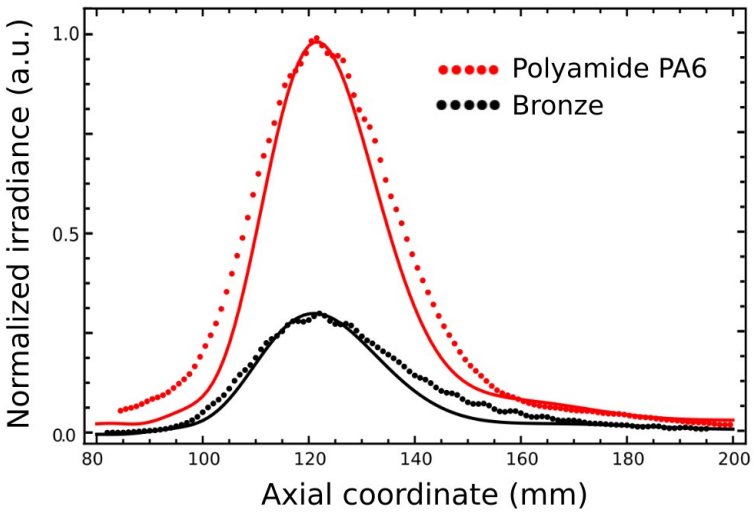

Fig. 2.25. Axial irradiances provided by the 3-D printed THz lenses shown in Fig 2.24. Experimental data are represented with dotted lines; and the corresponding numerical simulations by continuous lines. The maximum value of the irradiance for the PA6 lens was used for normalization.

The numerical simulations obtained with Eq. (1) are shown in the same Fig. for comparison (continuous lines). To obtain the numerical results, the transmittance of the lens was multiplied by the normalized field amplitude recorded of the at the lens plane (x,y) shown in Fig. 2.23.

In addition, we not considered a point-like detector as in Fig. 2.21c, but integrated the irradiance in the area of detection at the horn antenna. Note that, in spite of the surface roughness, and microstructure of the 3D printed lenses have not been considered, we found a very good agreement between theory and experiment. As expected phase polyamide TS is four times more efficient than the amplitude bronze TS of the same dimensions.

Conclusion

By using 3D printing technology, we have demonstrated the feasibility of realizing TS diffractive lenses. The focusing properties of both: amplitude and phase TS were tested using 0.625 THz beam. We have shown that TS can achieve better resolution than binary FZP. Further improvements are expected with other exotic sieves distributions [Giménez06, Giménez07]. So, our proposal opens the possibility to use low cost optics for a wide range of THz applications. Two examples of special interest are THz astronomical telescopes where ultralarge space telescope primaries are necessary, preferably as a single membrane; i.e, with no supporting structure [Andersen05, Withington04] and THz compressive sensing, to achieve the precise focalization needed in a single pixel camera [watts14].

References.

[Andersen05] G. Andersen, “Large optical photon sieve", *Optical Letters* **30**, 2976–2978 (2005).

[Busch14] S. F. Busch, M. Weidenbach, M. Fey, F. Schäfer, T. Probst y M. Koch, “Optical properties of 3D printable plastics in the THz regime y their application for 3D printed THz optics", *Journal of Infrared, Millimeter, y Terahertz Waves* **35**, 993–997 (2014).

[Cao03] Q. Cao y J. Jahns, “Nonparaxial model for the focusing of high-numerical-aperture photon sieves", *Journal of the Optical Society of America A* **20**, 1005–1012 (2003).

[D’Auria15] M. D’Auria et al., “3-D printed metal-pipe rectangular waveguides", *IEEE Transactions on Components, Packaging y Manufacturing* **5**, 1339–1349 (2015).

[Furlan16] W. D. Furlan, V. Ferrando, J. A. Monsoriu, P. Zagrajek, E. Czerwińska, y M. Szustakowski, “3D printed diffractive terahertz lenses", *Optical Letters* **41,** 1748–1751 (2016).

[Giménez06] F. Giménez, J. A. Monsoriu, W. D. Furlan, y A. Pons, “Fractal photon sieve", *Optics Express* **14**, 11958–11963 (2006).

[Giménez07] F. Giménez, W. D. Furlan, y J. A. Monsoriu, “Lacunar fractal photon sieves", *Optics Communications* **277**, 1–4 (2007).

[Kipp01] L. Kipp et al., “Sharper images by focusing soft x-rays with photon sieves", *Nature* **414**, 184–188 (2001).

[Liu16] C. Liu, L. Niu, K. Wang, y J. Liu, “3D-printed diffractive elements induced accelerating terahertz Airy beam", *Optics Express* **24**, 29342–29348 (2016).

[Menon05] R. Menon, D. Gil, G. Barbastathis, y H. Smith, “Photon-sieve lithography", *Journal of the Optical Society of America A* **22**, 342–345 (2005).

[Podzorov08] A. Podzorov y G. Gallot, “Low-loss polymers for terahertz applications", *Applied Optics* **47**, 3254–3257 (2008).

[Sabatyan11] A. Sabatyan y S. Mirzaie, “Efficiency-enhanced photon sieve using Gaussian/overlapping distribution of pinholes", *Applied Optics* **50**, 1517–1522 (2011).

[Scherger11] B. Scherger, M. Scheller, C. Jansen, M. Koch, y K. Wiesauer, “Terahertz lenses made by compression molding of micropowders”, *Applied Optics* **50**, 2256–2262 (2011).

[Sheppard88] C. J. R. Sheppard y Z. S. Hegedus “Axial behavior of pupil-plane filters", *Journal of the Optical Society of America A* **5**, 643–647 (1988).

[Siemion12] A. Siemion et al., “Diffractive paper lens for terahertz optics", *Optical Letters* **37**, 4320–4322 (2012).

[Squires15] A. D. Squires, E. Constable y A. Lewis, “3D printed terahertz diffraction gratings y lenses", *Journal of Infrared, Millimeter, y Terahertz Waves* **36**, 72–80 (2015).

[Suszek15] J. Suszek et al., “3-D-printed flat optics for THz linear scanners", *IEEE Transactions on Terahertz Science y Technology* **5**, 314–316 (2015).

[Wang02] S. Wang et al., “Characterization of T-ray binary lenses", *Optical Letters* **27**, 1183–1185, (2002).

[watts14] C. M. Watts et al., “Terahertz compressive imaging with metamaterial spatial light modulators", *Nature Photonics* **8**, 605–609 (2014).

[Wilk09] R. Wilk, N. Vieweg, O. Kopschinski y M. Koch, “Liquid crystal based electrically switchable Bragg structure for THz waves", *Optics Express* **17,** 7377–7382 (2009).

[Withington04] S. Withington, “Terahertz astronomical telescopes y instrumentation", *Philosophical Transactions of the Royal Society A: Mathematical, Physical y Engineering Sciences* **362**, 395–402 (2004).

[Yu09] Y. Yu y W. Dou, “Generation of pseudo-Bessel beams at THz frequencies by use of binary axicons", *Optics Express* **17**, 888–893 (2009).

2.5 Multiplexing THz vortex beams with a single diffractive 3D printed lens

Abstract

We present a novel method for experimentally generating multiplexed THz vortex beams by using a single 3D printed element that combines a set of radially distributed spiral phase plates, and a binary focusing Fresnel lens. With this element we have experimentally demonstrated that THz multiplexing can be tailored to fit within a small space on an optical bench. Results are presented beside numerical simulations, demonstrating the robust nature of the experimental method.

Introduction

The singular properties of terahertz radiation, such as good penetration and low scattering through various dielectric materials, non-ionizing photon energy, and broad spectral bandwidth, motivated the growing of THz photonics. Research in this field was benefited from the development of more efficient emitters, detectors, and optical components such as refractive and diffractive lenses, gratings, beam splitters, polarizers, and retarders [Mittleman03, Tonouchi07]. Recently, it has been demonstrated that even low cost 3D printing technology can be employed to construct non-conventional diffractive THz lenses [Wei15, Furlan16, Liu16, Furlan18, Mirzaei17]. In this way, technological improvements regarding THz beam shaping in the form of vortex beams, are of interest because, although such beams have found a

large number of applications in the visible domain (e.g., in sensing, microscopy and astronomical imaging, trapping and manipulating of matter, and communication technologies) [Roux04, Gbur06, Lee04, Tao06, Furlan09], few works have reported applications in the THz domain.

Vortex beams have orbital angular momentum and propagate with helical phase structure characterized by its azimuthally dependent phase $im\varphi$, in which φ is the transverse azimuthal coordinate and *m* is known as the topological charge. The fact that *m* can take any integer value motivated its use to encode and transmit information [Wan16]. Therefore, due to its high frequency, THz beams are good candidates for information carrier of the wireless communications. Moreover, vortex beams with different *m* values can be used as different carriers for multiplexing and transmitting different data streams along the same spatial axis improving the performance of communication systems using electromagnetic waves.

Successful methods used to obtain THz vortex beams include: off-axis holograms [Xie13], quarter-wave plate coupled to a wire polarizer [Imai14], arrays of wavelength-size V-shaped antennas [He13], binary phase axicons with spiral configuration of zones [Miyamoto14], and a photopatterned birefringence liquid crystal [Ge17]. However, most of these methods were demonstrated for single vortex beams. Since multiplexing several data channels has been used to significantly increase the data capacity in optical networks [Yu15, Lei15, Wan12], in this paper, we examine the creation of composite THz vortex beams representing a superposition of vortices with different topological charges. A multiplexing approach, known as space-division multiplexing [Li14], has been implemented to a multiplexed vortex THz lens (MVTL) using a 3D printer. The analysis of the THz vortices produced by this structure was performed experimentally, and numerically for comparison.

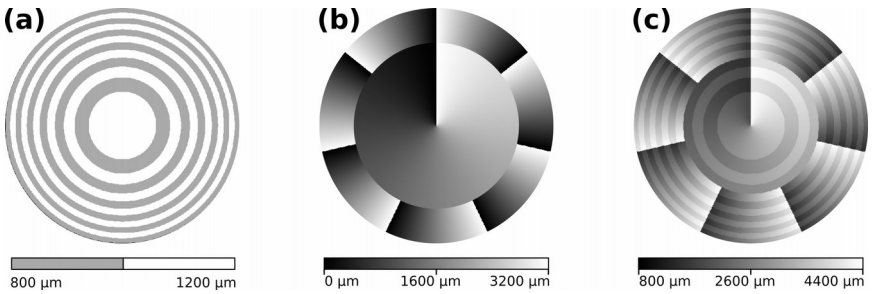

Fig. 2.26. Design of a multiplexed THz vortex lens. a) Base FZP using Eq.(1) with b) Multiplexed vortex SPP with topological charges inner part and outer part. c) Composite vortex lens as the superposition of a) and b). Gray levels represent the lens thickness to be constructed in PA6 polyamide by a 3D printer.

Design and construction

Our strategy for generating multiplexed THz vortex waves using a single element, consists on the combination of two elements represented as the product of two separable functions: one, having a radial dependence, is a conventional phase binary Fresnel zone plate whose radial phase dependence can be expressed as

$$\phi(r)=\pi\ rect[(r/a)^2-0.5]\ rect\left[\frac{mod[(r/a)^2+0.5\,p-1,p]}{p}\right] \quad (1)$$

where a is the radius of the zone p. The other element is a multiplexed spiral zone plate, which only has a phase dependence (linear) on the azimuthal angle. In this element N non-overlapping annular zones are arranged using the space division multiplexing technique.

$$\tau(\theta)=\begin{Bmatrix} m_1\theta, & 0\le r<r_1 \\ \dots & \\ m_j\theta, & r_{j-1}\le r<r_j \\ \dots & \\ m_N\theta, & r_{N-1}\le r<a \end{Bmatrix} \quad (2)$$

In this way the transmittance of the lens is given by $T(r,\theta)=e^{i\phi(r)\tau(\theta)}$.

As demonstration, we propose a MVTL that consists on the combination of two spiral phase functions with different topological charges m_1 and m_2, designed to work at 0.625 THz, and made of PA6 polyamide (absorption coefficient = 3.9 cm^{-1} and refractive index n=1.6).

The MVTL composition from its components is shown in Fig 2.26. On the one hand, the FZP (fig. 1a) was designed with alternate zones of thickness t_1=0.8 mm and t_2=1.2 mm which have been calculated to provide a πphase shift between the zones for the design wavelength of $\lambda=480\mu m)$, and using the following expression: $\Delta t=t_2-t_1=\lambda/2(n-1)$. On the other hand, the spatially multiplexed THz Spiral Phase Plate (SPP) (Fig. 2.26b) has two parts. The inner part, with topological charge $m_1=-1,$ is a circle of radius 7.33 mm that covers the 4 inner rings of the FZP. The outer part, with topological charge $m_2=7,$ has an annular shape with an outer radius 25.4 mm and covers from the 5th to the 12th of the FZP. In each part, the thickness of the SPP depends on the azimuthal angle around the center of the SPP, as

$$h(\theta)=mod(m\theta,2\pi)\frac{\lambda}{2\pi(n-1)} \quad (3)$$

Thus, a total phase shift of $|2\pi m|$, will be imprinted on the electromagnetic wave by each part of the SPP. Taking into account that this approach requires extreme precision in the pitch of helical surface, in order to reduce the fabrication errors we incremented

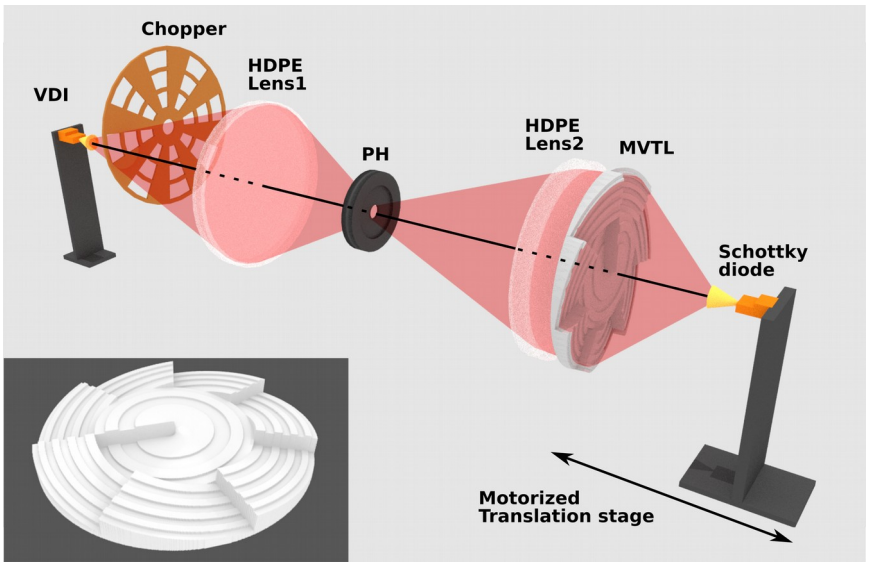

Fig. 2.27. Experimental setup for obtaining multiplexed THz vortex beams. The inset shows a CAD design of the MVTL experimental model.

the thickness in each point of the SPP by a constant factor $k=4$ providing an effective topological charge of km. In this way, for the plate in Fig. 2.26b $0 \leq h \leq 3.2\,mm$. Thus, the final THz design, shown in Fig. 2.26c, results as the superposition of the plates in Fig. 2.26a and Fig. 2.26b.

Experimental setup

The experimental setup for obtaining multiplexed THz vortex beams is shown in Fig. 2.27. A frequency multiplier based on Schottky diode (Virginia Diodes, Inc. Charlottesville, VA. USA), was used as a source of radiation. The source was equipped with a horn antenna which produced a divergent beam at 0.625 THz. The beam was focused on a pinhole (2 mm diameter) by a high density polyethylene (HDPE) refractive lens. Then, the

radiation was collimated, by a second HDPE lens, and directed onto the MVTL. The intensity distribution after the MVTL was scanned with a Schottky diode detector (Virginia Diodes, Inc. Charlottesville, VA. USA) also equipped with horn antenna (WR-1.5), having a 2.4 mm aperture diameter. The detector was mounted on a 3D motorized stage which allows high precision movement. To measure the signal from the detector, a lock-in system (Stanford Research Systems SR830), based on modulation at 187 Hz and a mechanical chopper, was used.

The inset in Fig. 2.27 shows the experimental model, which was designed using a CAD software (blender.org) and constructed with a 0.3 mm spatial resolution by an online 3D printing service (i.materialise, Leuven, Belgium). The MVTL was made from a polyamide granular powder by selective laser sintering technique. The diameter of the constructed lens was 50.8 mm, and the FZP has the main focal distance (first diffraction order) of 112 mm.

Results

Beam transverse irradiance profiles provided by the composite helical beam were recorded after the MVTL, along the optical axis in 1 mm intervals with an accuracy of 2 μm. Experimental results at five different planes are shown in Fig. 2.28 in comparison with numerical results computed using the Fresnel-Kirchoff nonparaxial scalar diffraction theory [6].

As expected the two main vortices are in focus at the FZP focal distance, the inner vortex corresponds to the $m_1=-1$ topological charge, while the outer vortex corresponds to the $m_2=7$ topological charge. The last one also exhibits a complex structure with a cosenoidal azimuthal variation. In fact, $k(m_2-m_1)=32$ lobes appear, as it was expected by the theoretical analysis [Bouchal07].

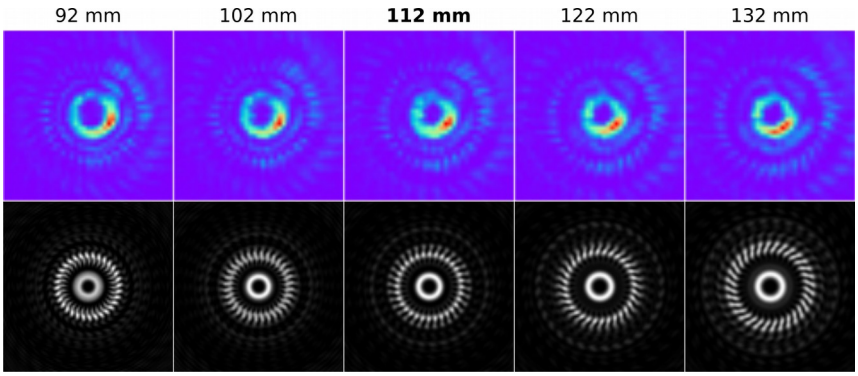

Fig. 2.28. Experimental results (upper row) and the numerical simulations (lower row) computed using Fresnel-Kirchof non-paraxial scalar difraction theory at diferent transverse planes around the FZL focal plane(z=112 mm).

spite of the differences between the physical lens and the theoretical design, due to the limitations of the 3D printer resolution (especially near the center of the plate), a very good agreement between theory and experiment can be appreciated in Fig. 2.28. Additional vortices, seen in the experimental results, are the consequence of non-integer steps heights of the lens designed for only one spectral component. Other sources of discrepancy between experimental and theoretical results are the inhomogeneities of the index of refraction and the finite size of the lens. Multiple reflections and standing waves in the MVTL, may also lead to azimuthal modulations in intensity [Berry04].

Conclusions

We have demonstrated the feasibility of realizing THz multiplexed vortex beams, with 3D printing technology. PA6 phase lenses were constructed and tested using 0.625 THz beam in a simple experimental THz setup. The experimental results were in good agreement with the simulations despite some sources of errors, demonstrating the robustness of our proposal. In this way,

this work extends to the THz domain previous use of phase optical elements in the visible domain [Guo04] that could find many applications in THz technologies. For instance, there have been recent growing interest in applying vortex beams to wireless communications [Willner15] and through mode multiplexing, vortex beams can tremendously increase the capacity of communication systems.

These novel techniques, developed for utilizing THz spectrum can be improved to achieve very high efficiency. In this sense, it has been demonstrated that dependencies of the vortex radius and width on topological charge can be controlled [Guo04], and, therefore, multiplexed THz vortex rings can be produced efficiently.

Acknowledgments

This study was supported by the Ministerio de Economía y Competitividad and FEDER (DPI2015-71256-R), Spain, and by the Generalitat Valenciana, (PROMETEO II-2014-072), Spain.

Partial support by the National Center for Research and Development in Poland (LIDER/020/319/L-5/13/NCBR/2014) is also acknowledged.

Federico Machado has been supported by the MayaNet - Erasmus Mundus Partnership 552061-EM-1-2014-1-IT-ERA MUNDUS-EMA21 (2014-0872/001-001).

References.

[Berry04] M. V. Berry, “Optical vortices evolving from helicoidal integer y fractional phase steps", *Journal of Optics A: Pure Applied Optics* **6**, 259-268 (2004).

[Bouchal07] Z. Bouchal, V. Kollarova, P. Zemanek, y T. Cizmar, “Orbital angular momentum of mixed vortex beams", *Proceedings of SPIE* **660907**, 1–8 (2007).

[Furlan09] W. D. Furlan, F. Giménez, A. Calatayud, y J. A. Monsoriu, "Devil's vortex-lenses", *Optics Express* **17**, 21891-21896 (2009).

[Furlan16b] W. D. Furlan, V. Ferrando, J. A. Monsoriu, P. Zagrajek, E. Czerwinska, y M. Szustakowski, "3D printed diffractive terahertz lenses", *Optical Letters* **41**, 1748-1751 (2016).

[Furlan18] W. D. Furlan, F. Machado, J. A. Monsoriu, y P. Zagrajek, "Terahertz Sieves", *IEEE Transactions on Terahertz Science y Technology* **8**, 140-143 (2018).

[Gbur06] G. Gbur, y T. D. Visser, "Phase singularities y coherence vortices in linear optical systems", *Optics Communications* **259**, 428–435 (2006).

[Ge17] S. Ge, P. Chen, Z. Shen, W. Sun, X. Wang, W. Hu, Y. Zhang, y Y. Lu, "Terahertz vortex beam generator based on a photopatterned large birefringence liquid crystal", *Optics Express* **25**, 12349-12356 (2017).

[Guo04] C. S. Guo, X. Liu, J. L. He, y H. T. Wang, "Optimal annulus structures of optical vortices", *Optics Express* **12**, 4625-4634 (2004).

[He13] J. He, X. Wang, D. Hu, J. Ye, S. Feng, Q. Kan, y Y. Zhang, "Generation y evolution of the terahertz vortex beam", *Optics Express* **21**, 20230-20239 (2013).

[Imai14] R. Imai, N. Kanda, T. Higuchi, K. Konishi, y M. Kuwata-Gonokami, "Generation of broadby terahertz vortex beams", *Optical Letters* **39**, 3714-3717 (2014).

[Lee04] W. M. Lee, X. C. Yuan, y W. C. Cheong, "Optical vortex beam shaping by use of highly efficient irregular spiral phase plates for optical micromanipulation", *Optical Letters* **29**, 1796–1798 (2004).

[Lei15] T. Lei, M. Zhang, Y. R. Li, P. Jia, G. N. Liu, X. G. Xu, Z. H. Li, C. J. Min, J. Lin, C. Y. Yu, H. B. Niu, y X. C. Yuan, "Massive individual orbital angular momentum channels for multiplexing enabled by Dammann gratings", *Light: Science & Applications* **4**, e257 (2015).

[Li14] G. Li, N. Bai, N. Zhao, y C. Xia, "Space-division multiplexing: the next frontier in optical communication", *Advances in Optics y Photonics* **6**, 413-487 (2014).

[Liu16] C. Liu, L. Niu, K. Wang, J. Liu, "3D-printed diffractive elements induced accelerating terahertz Airy beam", *Optics Express* **24**, 29342-29348 (2016).

[Mirzaei17] B. Mirzaei, J. R. G. Silva, Y. C. Luo, X. X. Liu, L. Wei, D. J. Hayton, … , y C. Groppi, "Efficiency of multi-beam Fourier phase gratings at 1.4 THz", *Optics Express* **25**, 6581-6588 (2017).

[Mittleman03] D. Mittleman, Sensing with Terahertz Radiation (Springer, Berlin, 2003).

[Miyamoto14] K. Miyamoto, K. Suizu, T. Akiba, y T. Omatsu, “Direct observation of the topological charge of a terahertz vortex beam generated by a Tsurupica spiral phase plate", *Applied Physics Letters* **104**, 261104 (2014).

[Roux04] F. S. Roux, “Distribution of angular momentum y vortex morphology in optical beams", *Optics Communications* **242**, 45–55 (2004).

[Tao06] S. H. Tao, X.-C. Yuan, J. Lin, y R. Burge, “Sequence of focused optical vortices generated by a spiral fractal zone plates", *Applied Physics Letters* **89**, 031105 (2006).

[Tonouchi07] M. Tonouchi, “Cutting-edge terahertz technology", *Nature Photonics* **1**, 97–105 (2007).

[Wan12] J. Wang, J. Y. Yang, I. M. Fazal, N. Ahmed, Y. Yan, H. Huang, Y. Ren, Y. Yue, S. Dolinar, M. Tur, y A. E. Willner, “Terabit freespace data transmission employing orbital angular momentum multiplexing", *Nature Photonics* **6**, 488–496 (2012).

[Wan16] J. Wang, "Advances in communications using optical vortices", *Photonics Research* **4**, B14-B28 (2016).

[Wei15] X. Wei, C. Liu, L. Niu, Z. Zhang, K. Wang, Z. Yang, y J. Liu, “Generation of arbitrary order Bessel beams via 3D printed axicons at the terahertz frequency range", *Applied Optics* **54**, 10641–10649 (2015).

[Willner15] A. E. Willner, et al., “Optical communications using orbital angular momentum beams", *Advances in Optics y Photonics* **7**, 66–106 (2015).

[Xie13] Z. Xie, X. Wang, J. Ye, S. Feng, W. Sun, T. Akalin, y Y. Zhang, “Spatial terahertz modulator", *Scientific Reports* **3**, 3347 (2013).

[Yu15] S. Yu, “Potentials y challenges of using orbital angular momentum communications in optical interconnects", *Optics Express* **23**, 3075–3087 (2015).

Capítulo 3

Discusión general de los resultados

En este capítulo se hace una reflexión general de los resultados alcanzados. Cabe destacar que estos resultados han sido obtenidos tras tres años de investigación en el marco de una beca de doctorado internacional Erasmus Mundus MAYANET.

Como se ha podido comprobar a lo largo de la presente memoria, esta Tesis se enmarca en el estudio de EODs basadas en secuencias aperiódicas como son el conjunto fractal de Cantor, las secuencias de *m*-bonacci (Fibonacci, Tribonacci, Tetranacci, …) y las funciones radiales de Walsh. En concreto, el trabajo se centra en el diseño y caracterización experimental de PZs cuya transmitancia a lo largo de la variable radial cuadrática se basa en estas secuencias aperiódicas. Adicionalmente, también se ha abarcado el diseño y construcción de prototipos de diferentes lentes difractivas para la focalización de haces de THz.

El punto de partida de esta Tesis Doctoral lo constituyó el capítulo del libro “Fractal Light Vortices” que recoge el estado del arte relacionado con las lentes-vortice fractales [Calatayud12, Furlan09, Furlan10]. Estas lentes combinan PZFs [Furlan03b, Furlan04, Furlan05, Furlan07, Giménez10, Saavedra03] basadas en el conjunto de Cantor con máscaras de fase helicoidales de diferente carga topológica [Calatayud13, Furlan09]. Al ser iluminadas por una onda plana generan un volumen focal autosimilar con múltiples vórtices ópticos que potencialmente

podrán ser utilizadas en el diseño de nuevas trampas ópticas para la manipulación de micropartículas.

Junto al conjunto fractal de Cantor, la secuencia de Fibonacci también había sido implementada en el diseño de lentes difractivas aperiódicas [Calatayud13, Ferrando14, Monsoriu13]. En esta Tesis se dio un paso adicional con la secuencia generalizada de *m*-bonacci, siendo Fibonacci un caso particular para $m=2$. En el artículo "Diffractive *m*-bonacci zone plates" se analizó en profundidad, tanto numérica como experimentalmente los casos $m=3$ (Tribonacci) y $m=4$ (Tetranacci). Respecto a las PZs periódicas equivalentes, se obtuvieron en ambos casos dos focos a lo largo del eje óptico, siendo la relación de las correspondientes distancias focales igual a la proporción áurea generalizada.

Si con la secuencia de *m*-bonacci se pueden diseñar lentes difractivas bifocales, en el artículo "Multiple-plane image formation by Walsh zone plates" hemos comprobado que es posible implementar lentes difractivas cuatrifocales utilizando las funciones radiales de Walsh. Estas funciones aperiódicas ya habían sido consideradas previamente en el diseño de filtros ópticos [Hazra07, Mukherjee14a, Mukherjee14b]. Como PZs aperiódicas, es decir como PZs cuya transmitancia radial cuadrática viene dada por funciones de Walsh, hemos demostrado que se comportan como lentes difractivas cuatrifocales. Además, la distribución e intensidad relativa de sus focos se puede controlar con una selección adecuada de los parámetros de diseño. Por lo tanto, las lentes difractivas de Walsh abren un nuevo abanico de posibles aplicaciones tecnológicas. Por ejemplo, podrían ser utilizadas en el diseño de lentes de contacto o intraoculares difractivas multifocales.

Tras el estudio de todas estas EODs en el rango visible, la siguiente etapa de la Tesis se centró en el estudio de diferentes PZs en el rango de los THz [Furlan16]. En el artículo "Terahertz

Sieves" se presentaron las primeras CFs desarrolladas para la focalización y formación de imágenes en este rango espectral. La construcción de prototipos de estas lentes difractivas mediante impresión 3D permitió comprobar experimentalmente las propiedades de focalización y se compararon satisfactoriamente con los cálculos numéricos obtenidos mediante las ecuaciones de propagación no paraxial. Al igual que en el rango visible, se pudo verificar que una CFs también produce una apodización de los focos de orden superior cuando trabajan en el rango de los THz.

Finalmente, en la publicación "Multiplexing THz vortex beams with a single diffractive 3D printed lens" se propuso el multiplexado de vórtices en el rango de los THz. También se construyeron prototipos mediante impresión 3D combinando en una misma lente difractiva dos cargas topológicas en diferentes sectores radiales. Esta combinación permite la focalización de haces de THz en dos vórtices concéntricos, lo que podría ser utilizado para incrementar la capacidad de sistemas de comunicaciones mediante el multiplexado de vórtices [Willner15].

Capítulo 4

Conclusiones

En este capítulo se revisa el nivel de cumplimiento de los objetivos de esta Tesis Doctoral expuestos en la introducción. También se describen las principales aportaciones realizadas en el diseño y caracterización experimental de los nuevos EODs. Finalmente, se proponen diversas líneas de investigación futuras.

El primer objetivo que consistía en el *Diseño y optimización de elementos ópticos difractivos multifocales basados en secuencias aperiódicas*, ha sido alcanzado con los EODs presentados en las publicaciones 1, 2 y 3. En concreto, se han analizado y caracterizado experimentalmente diferentes lentes difractivas basadas en el conjunto fractal de Cantor (publicación 1), en las funciones radiales de Walsh (publicación 2) y en la secuencia generalizada de *m*-bonacci (publicación 3). Especialmente interesantes resultan las lentes de Walsh como nuevas lentes difractivas cuatrifocales.

El segundo objetivo, *Diseño y modelización de elementos ópticos difractivos con diferentes cargas topológicas* se ha logrado, tanto en el rango visible en la publicación 1, como en el rango de los THz en la publicación 5. En este último caso, se ha considerado además la combinación de dos cargas topológicas diferentes en un mismo EOD, lo que ha permitido la generación de vórtices concéntricos.

En cuanto al tercer y último objetivo, *Diseño, construcción de prototipos y caracterización experimental de lentes difractivas en el rango de los THz*, en las publicaciones 4 y 5 se han realizado

diferentes prototipos de estas lentes mediante técnicas de impresión 3D, una tecnología de bajo coste que está en pleno proceso de expansión.

Finalmente se proponen varias líneas de investigación futuras relacionadas con las obtenidas en la Tesis Doctoral. En primer lugar se pretende seguir diseñando lentes basadas en otras secuencias aperiódicas (Rudin-Shapiro, Paper folding, Silver mean ...) en búsqueda de nuevas propiedades de focalización y formación de imágenes. También se analizarán la combinación de varias de estas secuencias en una misma lente difractiva para la obtención de nuevas distribuciones de irradiancia, o la combinación con máscara de fase helicoidales para la generación de nuevas lentes-vórtice aperiódicas.Todas estas estructuras serán analizadas tanto teórica como experimentalmente utilizando una pantalla de cristal líquido.

Por otra parte, se pretende continuar con la construcción de lentes difractivas en el rango de los THz mediante técnicas de impresión 3D. Se prestará especial interés a las secuencias aperiódicas indicadas anteriormente analizando si sus propiedades de focalización y formación de imágenes son extrapolables al rango de los THz.

Bibliografía general

[Allen99] L. Allen, M. J. Padgett y M. Babiker, “The orbital angular momentum of light”, *Progress in Optics* **39**, 291–372 (1999).

[Andersen05] G. Andersen, “Large optical photon sieve”, *Optics Letters* **30**, 2976–2978 (2005).

[Astley10] V. Astley, J. Scheiman, R. Mendis y D. M. Mittleman, “Bending and coupling losses in terahertz wire waveguides”, *Optical Letters* **35**, 553 (2010).

[Barrera12] J. F. Barrera, M. Tebaldi, D. Amaya, W. D. Furlan, J. A. Monsoriu, N. Bolognini, y R. Torroba, “Multiplexing of encrypted data using fractal masks", *Optical Letters* **37**, 2895–2897 (2012).

[Basin63] S. L. Basin, “The Fibonacci sequence as it appears in nature”, *Fibonacci Quarterly* **1**, 53–56(1963).

[Beauchamp84] K.G. Beauchamp, *Applications of Walsh y related functions*, Academic Press, London (1984).

[Bekshaev08] A. Bekshaev, M. Soskin y M. Vasnetsov, *Paraxial Light Beams with Angular Momentum*, Nova Publishers (2008)

[Berry04] M. V. Berry, “Optical vortices evolving from helicoidal integer y fractional phase steps", *Journal of Optics A: Pure Applied Optics* **6**, 259-268 (2004).

[Bishop03] A. Bishop, T. Nieminen, N. Heckenberg y H. Rubinsztein-Dunlop, “Optical application and measurement of torque on microparticles of isotropic nonabsorbing material”, *Physical Review* A **68**, 033802 (2003).

[Bouchal04] Z. Bouchal y R. Čelechovský, “Mixed vortex states of light as information carriers”, *New Journal of Physics* 6, 1-15 (2004).

[Bouchal07] Z. Bouchal, V. Kollarova, P. Zemanek, y T. Cizmar, “Orbital angular momentum of mixed vortex beams", *Proceedings of SPIE* **660907**, 1–8 (2007).

[Brasselet09] E. Brasselet, N. Murazawa, H. Misawa y S. Juodkazis, “Optical vortices from liquid crystal droplets”, *Physical Review Letters* **103**, 103903 (2009).

[Busch14] S. F. Busch, M. Weidenbach, M. Fey, F. Schäfer, T. Probst y M. Koch, “Optical properties of 3D printable plastics in the THz regime y their application for 3D printed THz optics", *Journal of Infrared, Millimeter, y Terahertz Waves* **35**, 993–997 (2014).

[Calabuig13] A. Calabuig, S. Sánchez-Ruiz, L. Martínez-León, E. Tajahuerce, M. Fernández-Alonso, W. D. Furlan, J. A Monsoriu, y A. Pons-Martí, “Generation of programmable 3D optical vortex structures through devil’s vortex-lens arrays", *Applied Optics* **52**, 5822–5829 (2013).

[Calatayud12] A. Calatayud, J. A. Rodrigo, L. Remón, W. D. Furlan, G. Cristóbal y J. A. Monsoriu, “Experimental generation y characterization of Devil’s vortex-lenses”, *Applied Physics B* **106**, 915–919 (2012).

[Calatayud13a] A. Calatayud, V. Ferrando, L. Remón, W. D. Furlan y J. A. Monsoriu, “Twin axial vortices generated by Fibonacci lenses”, *Optics Express* **21**, 10234–10239 (2013).

[Calatayud13b] A. Calatayud, V. Ferrando, F. Giménez, W. D. Furlan, G. Saavedra y J.A. Monsoriu, “Fractal square zone plates”, *Optics communications* **286**, 42-45 (2013).

[Cao02] Q. Cao y J. Jahns, “Focusing analysis of the pinhole photon sieve: Individual far-field model”, *Journal of the Optical Society of America* **19**, 2387–2393 (2002).

[Cao03] Q. Cao y J. Jahns, “Nonparaxial model for the focusing of high-numerical-aperture photon sieves", *Journal of the Optical Society of America A* **20**, 1005–1012 (2003).

[Cheng16] S. Cheng, X. Zhang, W. Ma, y S. Tao, “Fractal zone plate beam based optical tweezers", *Scientific Reports* **6**, 34492 (2016).

[Curtis02] J. E. Curtis, A. K. Brian y D. G. Grier, “Dynamic holographic optical tweezers”, *Optics Communications* **207**, 169-175 (2002).

[D’Auria15] M. D’Auria et al., “3-D printed metal-pipe rectangular waveguides", *IEEE Transactions on Components, Packaging y Manufacturing* **5**, 1339–1349 (2015).

[Dai08] H. Dai, J. Liu, S. Xuecheng, y Y. Dejin, “Programmable fractal zone plates (FraZPs) with foci finely tuned", *Optics Communications* **281**, 5515–5519 (2008)

[Davis04] J. A. Davis, L. Ramirez, J. A. Rodrigo Martín-Romo, T. Alieva y M. L. Calvo, “Focusing properties of fractal zone plates: Experimental implementation with a liquid-crystal display", *Optics Letters* **29**, 1321–1323 (2004).

[Desyatnikov15] A. Desyatnikov, Y. Kivshar y L. Torner, “Optical vortices y vortex solitons”, *Progress in Optics* **47**, 291–391 (2005).

[Ferrando13] V. Ferrando, A. Calatayud, F. Giménez, W. D. Furlan, y J. A. Monsoriu, “Cantor dust zone plates", Optics Express **21**, 2701–2706 (2013).

[Ferrando14] V. Ferrando, A. Calatayud, P. Andrés, R. Torroba, W. D. Furlan y J. A. Monsoriu, “Imaging Properties of Kinoform Fibonacci Lenses”, *IEEE Photonics Journal* **6**, 6500106 (2014).

[Ferrando15] V. Ferrando, F. Giménez, W. D. Furlan y J. A. Monsoriu, “Bifractal focusing y imaging properties of Thue-Morse Zone Plates", *Optics Express* **23**, 19846–19853 (2015).

[Fleming02] A. J. Fleming, “Plant mathematics and Fibonacci’s flowers”, *Nature* **418**, 723 (2002).

[Friese01] M. Friese, H. Rubinsztein-Dunlop, J. Gold, P. Hagberg y D. Hanstorp, “Optically driven micromachine elements”, *Applied Physics Letters* **78,** 547–549 (2001).

[Furlan03a] W.D.Furlan, G. Saavedra, J.A.Monsoriu, “Fractal zone plates” *Optical letters* **12**, 971-973 (2003).

[Furlan03b] W.D.Furlan, G. Saavedra, J.A.Monsoriu, “Fractal zone plates produce axial irradiance with fractal profile”, Optics & Photonics news **31** (2003).

[Furlan04] W.D.Furlan, G. Saavedra, J.A.Monsoriu, “Fractal zone plates with variable lacunarity”

[Furlan05] W.D.Furlan, G. Saavedra, J.A.Monsoriu, “Focusing light with fractal zone plates”, *E.DO.* **5**, 001-0015 (2005).

[Furlan07] W. D. Furlan, G. Saavedra y J. A. Monsoriu, “White light imaging with fractal zone plates", *Optics Letters* **32**, 2109– 2111 (2007).

[Furlan09] W. D. Furlan, F. Giménez, A. Calatayud y J. A. Monsoriu, “Devil’s vortex-lenses”, *Optics Express* **17**, 21891–21896 (2009)

[Furlan10] W. D. Furlan, F. Giménez, A. Calatayud, L. Remón y J. A. Monsoriu, “Volumetric multiple optical traps produced by Devil's lenses”, *Journal of the European Optical Society-Rapid Publications* **5**, 10037s (2010).

[Furlan16] W. D. Furlan, V. Ferrando, J. A. Monsoriu, P. Zagrajek, E. Czerwińska, y M. Szustakowski, “3D printed diffractive terahertz lenses", *Optical Letters* **41,** 1748–1751 (2016).

[Furlan18] W. D. Furlan, F. Machado, J. A. Monsoriu, y P. Zagrajek, “Terahertz Sieves", *IEEE Transactions on Terahertz Science y Technology* **8**, 140-143 (2018).

[Gahagan96] K. T. Gahagan y G. A. Swartzlander, “Optical vortex trapping of particles”, *Optics Letters* **21**, 827 (1996)

[Gao11] N. Gao, Y. Zhang, y C. Xie, “Circular Fibonacci gratings", *Applied Optics* **50**, G142–G148 (2011).

[Garcés-Chávez02] V. Garcés-Chávez, K. Volke-Sepulveda, S. Chávez-Cerda, W. Sibbett y K. Dholakia, “Transfer of orbital angular momentum to an optically trapped low-index particle”, *Physics Review A* **66**, 063402 (2002)

[García-Martínez12] P. García-Martínez, M. M. Sánchez-López, J. A. Davis, D. M. Cottrell, D. Sy e I. Moreno, “Generation of Bessel beam arrays through Dammann gratings”, *Applied Optics* **51**, 1375–1381 (2012).

[Garland87] Garly T. H., *Fascinating Fibonaccis: Mystery y Magic in Numbers*, Dale Seymour Publications (1987).

[Gbur06] G. Gbur, y T. D. Visser, “Phase singularities y coherence vortices in linear optical systems", *Optics Communications* **259**, 428–435 (2006).

[Ge12] X. Ge, Z. Wang, K. Gao, D. Wang, Z. Wu, J. Chen, Z. Pan, K. Zhang, Y. Hong, P. Zhu y Z. Wu, “Use of fractal zone plates for transmission X-ray microscopy”, *Analytical and bioanalytical chemistry* **404**, 1303–1309 (2012).

[Ge17] S. Ge, P. Chen, Z. Shen, W. Sun, X. Wang, W. Hu, Y. Zhang, y Y. Lu, “Terahertz vortex beam generator based on a photopatterned large birefringence liquid crystal", *Optics Express* **25**, 12349-12356 (2017).

[Gibson04] G. Gibson, J. Courtial, M. Padgett, M. Vasnetsov y V. Pasco, “Free-space information transfer using light beams carrying orbital angular momentum”, *Optical Express* **12**, 5448-5456 (2004).

[Giménez06] F. Giménez, J. A. Monsoriu, W. D. Furlan, y A. Pons, “Fractal photon sieve", *Optics Express* **14**, 11958–11963 (2006).

[Giménez07] F. Giménez, W. D. Furlan, y J. A. Monsoriu, “Lacunar fractal photon sieves", *Optics Communications* **277**, 1–4 (2007).

[Giménez10] F. Giménez, W. D. Furlan, A. Calatayud, y J. A. Monsoriu, “Multifractal zone plates", *Journal of the Optical Society of America A* **27**, 1851–1855 (2010)

[Grier03] D. G. Grier, “A revolution in optical manipulation”, **424**, 810–816 (2003).

[Guo04] C. S. Guo, X. Liu, J. L. He, y H. T. Wang, "Optimal annulus structures of optical vortices", *Optics Express* **12**, 4625-4634 (2004).

[Harmuth69] H.F. Harmuth, “Applications of Walsh functions in communications", *IEEE Spectrum* **6**, 82–91 (1969).

[Hazra07] L.N. Hazra, “Walsh filters for tailoring of resolution in microscopic imaging", *Micron* **38**(2), 129–135 (2007).

[Hazra76] L.N. Hazra y A. Banerjee, “Applications of Walsh functions in generation of optimum apodizers", *Journal of Optics* **5**, 19–26 (1976).

[Hazra77] L.N. Hazra, “A new class of optimum amplitude filters", *Optics Communications* **21**, 232–236 (1977).

[He13] J. He, X. Wang, D. Hu, J. Ye, S. Feng, Q. Kan, y Y. Zhang, “Generation y evolution of the terahertz vortex beam", *Optics Express* **21**, 20230-20239 (2013).

[Herrmannsfeldt68] W.B. Herrmannsfeldt, M.J. Lee, J.J. Spranza y K.R. Triggers, “Precision Alignment Using a System of Large Rectangular Fresnel Lenses”, *Applied Optics* **7,** 995-1005 (1968).

[Hsueh14] W. J. Hsueh, C. H. Chang y C. T. Lin, “Exciton photoluminescence in resonant quasi-periodic Thue-Morse quantum wells”, *Optical Letters* **39**, 489–492 (2014).

[Huang13] H. Huang, D. Liu, H. Zhang y X. Kong, “Electronic transport and shot noise in Thue-Morse sequence graphene superlattice", Journal of Applyed Physics. **113**, 043702 (2013).

[Imai14] R. Imai, N. Kanda, T. Higuchi, K. Konishi, y M. Kuwata-Gonokami, ”Generation of broadby terahertz vortex beams", *Optical Letters* **39**, 3714-3717 (2014).

[Ji18] Z. Ji, H. Zang, C. Fan, J. Wang, C. Zheng, L. Wei, C. Wang y L. Cao, “Fractal spiral zone plates”. *Journal of the Optical Society of America A*

[Ke15] J. Ke y J. Zhang, “Generalized Fibonacci photon sieves", *Applied Optics* **54**, 7278–7283 (2015).

[Kipp01] L. Kipp et al., “Sharper images by focusing soft x-rays with photon sieves", *Nature* **414**, 184–188 (2001).

[Ladavac04] K. Ladavac and D. G. Grier, “Microoptomechanical pumps assembled and driven by holographic optical vortex arrays”, *Optics Express* **12**, 1144–1149 (2004).

[Lee04] W. M. Lee, X. C. Yuan, y W. C. Cheong, “Optical vortex beam shaping by use of highly efficient irregular spiral phase plates for optical micromanipulation", *Optical Letters* **29**, 1796–1798 (2004).

[Lee06] J. H. Lee, G. Foo, E. G. Johnson y G. A. Swartzlander, “Experimental verification of an optical vortex coronagraph”, *Physics Review Letters* **97**, 053901(2006).

[Lei15] T. Lei, M. Zhang, Y. R. Li, P. Jia, G. N. Liu, X. G. Xu, Z. H. Li, C. J. Min, J. Lin, C. Y. Yu, H. B. Niu, y X. C. Yuan, “Massive individual orbital angular momentum channels for multiplexing enabled by Dammann gratings", *Light: Science & Applications* **4**, e257 (2015).

[Li14] G. Li, N. Bai, N. Zhao, y C. Xia, "Space-division multiplexing: the next frontier in optical communication", *Advances in Optics y Photonics* **6**, 413-487 (2014).

[Linage06] G. Linage, F. Montoya, A. Sarmiento, K. Showalter y P. Parmananda, “Fibonacci order in the period-doubling cascade to chaos”, *Physics Letters* **359**, 638–639 (2006).

[Liu16] C. Liu, L. Niu, K. Wang, y J. Liu, “3D-printed diffractive elements induced accelerating terahertz Airy beam", *Optics Express* **24**, 29342–29348 (2016).

[Lusk01] D. Lusk, I. Abdulhalim y F. Placido, “Omnidirectional reflection from Fibonacci quasi-periodic one-dimensional photonic crystal. Optics Communications”, **198**, 273–279 (2001).

[Maciá06] E. Maciá, “The role of aperiodic order in science y technology”, *Reports on Progress in Physics* **69**, 397-441 (2006).

[Maciá12] E. Maciá, “Exploiting aperiodic designs in nanophotonic devices”. *Reports in Progress on Physics* **75**, 1–42 (2012).

[Masajada01] J. Masajada y B. Dubik, “Optical vortex generation by three plane wave interference”, *Optics Communications* **198,** 21–27 (2001).

[Menon05] R. Menon, D. Gil, G. Barbastathis y H. I. Smith, “Photon-sieve lithography”, *Journal of the Optical Society of America A* **22**, 342–345 (2005).

[Mirzaei17] B. Mirzaei, J. R. G. Silva, Y. C. Luo, X. X. Liu, L. Wei, D. J. Hayton, … , y C. Groppi, “Efficiency of multi-beam Fourier phase gratings at 1.4 THz", *Optics Express* **25**, 6581-6588 (2017).

[Mittleman03] D. Mittleman, Sensing with Terahertz Radiation (Springer, Berlin, 2003).

[Miyamoto14] K. Miyamoto, K. Suizu, T. Akiba, y T. Omatsu, “Direct observation of the topological charge of a terahertz vortex beam generated by a Tsurupica spiral phase plate", *Applied Physics Letters* **104**, 261104 (2014).

[Mohacsi17] I. Mohacsi, I. Vartiainen, B. Rösner, M. Guizar-Sicairos, V.A. Guzenko, I. McNulty, R. Winarski, M.V. Holt y C. David, “Interlaced zone plate optics for hard X-ray imaging in the 10 nm range", *Scientific Reports* **7**, 43624 (2017).

[Monsoriu03] J. A. Monsoriu, E. Silvestre, A. Ferrando, P. Andrés y J. J. Miret, “High-index-core Bragg fibers: dispersion properties”, *Optics Express* **11**, 1400–1405 (2003).

[Monsoriu04] J. A. Monsoriu, G. Saavedra y W. D. Furlan, “Fractal zone plates with variable lacunarity", *Optics Express* **12**, 4227–4234 (2004).

[Monsoriu06] J. A. Monsoriu, C. J. Zapata-Rodriguez y W. D. Furlan, “Fractal axicons", *Optics Communications* **263**, 1–5 (2006)

[Monsoriu07a] J. A. Monsoriu, W. D. Furlan, G. Saavedra y F. Giménez, “Devil’s lenses”, Optics Express **15**, 13858–13864 (2007).

[Monsoriu07b] J. A. Monsoriu, R. A. Depine y E. Silvestre, “Non-Bragg by gaps in 1D metamaterial aperiodic multilayers”, *Optics Express* **2**, 07002 (2007).

[Monsoriu13] J. A. Monsoriu, A. Calatayud, L. Remon, W. D. Furlan, G. Saavedra y P. Andrés, “Bifocal Fibonacci diffractive lenses", *IEEE Photonics Journal* **5**, 3400106 (2013).

[Monsoriu15] J. A. Monsoriu, M. H. Giménez, W. D. Furlan, J. C. Barreiro, y G. Saavedra, “Diffraction by m-bonacci gratings", *European Journal of Physics* **36**, 65005 (2015).

[Mukherjee14a] P. Mukherjee y L.N. Hazra, “Self-similarity in radial Walsh filters y axial intensity distributions in the far-field diffraction patterns", *Journal of Optical Society of America* **31**, 379–387 (2014).

[Mukherjee14b] P. Mukherjee y L.N. Hazra, “Self-similarity in transverse intensity distributions in farfield diffraction patterns of radial Walsh filters", *Advances in Optics* **2014**, 352316 (2014).

[Noe] T. Noe, T. Piezas, y E. W. Weisstein, “Fibonacci n-Step Number", From MathWorld–A Wolfram WebResource. http://mathworld.wolfram.com/Fibonaccin-StepNumber

[Ojeda-Castañeda96] J. Ojeda-Castaneda y C. Gomez-Reino, “Selected Papers on Zone Plates”, *SPIE Optical Engineering Press* **MS128**, 512-518 (1996).

[Podzorov08] A. Podzorov y G. Gallot, “Low-loss polymers for terahertz applications", *Applied Optics* **47**, 3254–3257 (2008).

[Pu15] J. Pu y P. H. Jones, “Devil’s lens optical tweezers", *Optics Express* **23**, 8190–8199 (2015).

[Reicherter99] M. Reicherter, T. Haist, E. Wagemann y H. Tiziani, “Optical particle trapping with computer-generated holograms written on a liquid-crystal display”, *Optical Letters* **24**, 608–610 (1999),

[Remón13] L. Remón, A. Calatayud, V. Ferrando, W. D. Furlan y J. A. Monsoriu, “Chromatic behavior of multifocal intraocular lenses”, “X Congreso Nacional del Color”, 648–653, Valencia (2013).

[Roux04] F. S. Roux, “Distribution of angular momentum and vortex morphology in optical beams”, *Optical Communications* **242,** 45-55 (2004).

[Saavedra03] G. Saavedra, W. D. Furlan y J. A. Monsoriu, “Fractal zone plates”, *Optical Letters* **28**, 971-973 (2003).

[Sabatyan11] A. Sabatyan y S. Mirzaie, “Efficiency-enhanced photon sieve using Gaussian/overlapping distribution of pinholes", *Applied Optics* **50**, 1517–1522 (2011).

[Sah95] Y. Sah y G. Ranganath, “Optical diffraction in some Fibonacci structures”. *Optics Communications* **114**, 18–24 (1995).

[Sakdinawat07] A. Sakdinawat y Y. Liu, “Soft-x-ray microscopy using spiral zone plates”, *Optical Letters* **32**, 2635-2637 (2007).

[Scherger11a] B. Scherger, C. Jördens y M. Koch, “Variable-focus terahertz lens” *Optics Express* **19**, 4528 (2011).

[Scherger11b] B. Scherger, M. Scheller, C. Jansen, M. Koch y K. Wiesauer, “Terahertz lenses made by compression molding of micropowders”, *Applyed Optics* **50**, 2256 (2011).

[Shechtman84] D. Shechtman, I. Blech, D. Gratias y J. W. Cahn, “Metallic Phase with Long-Range Orientational Order and No Translational Symmetry”, *Physical Review Letters* **53**, 1951–1953 (1984).

[Sheppard88] C. J. R. Sheppard y Z. S. Hegedus “Axial behavior of pupil-plane filters", *Journal of the Optical Society of America A* **5**, 643–647 (1988).

[Siemion12] A. Siemion, M. Makowski, J. Suszek, J. Bomba, A. Czerwiski, F. Garet, J. L. Coutaz y M. Sypek, “Diffractive paper lens for terahertz optics”, *Optical Letters* **37**, 4320-4322 (2012).

[Spektor08] B. Spektor, A. Normatov y J. Shamir, “Singular beam microscopy”, *Applied Optics* **47**, A78 (2008)

[Squires15] A. D. Squires, E. Constable y A. Lewis, “3D printed terahertz diffraction gratings y lenses", *Journal of Infrared, Millimeter, y Terahertz Waves* **36**, 72–80 (2015).

[Suszek15] J. Suszek et al., “3-D-printed flat optics for THz linear scanners", *IEEE Transactions on Terahertz Science y Technology* **5**, 314–316 (2015).

[Swartzlander08] G. A. Swartzlander Jr, E. L. Ford, R. S. Abdul-Malik, L. M. Close y M. A. Peters, “Astronomical demonstration of an optical vortex coronagraph”, *Optical Express* **16**. 10200–10207 (2008).

[Tao06] S. H. Tao, X. C. Yuan, J. Lin y R. Burge, “Sequence of focused optical vortices generated by a spiral fractal zone plates”, *Applied Physics Letters* **89**, 031105 (2006).

[Tao13] S. H. Tao, B. C. Yang, H. Xia, y W. X. Yu, “Tailorable three-dimensional distribution of laser foci based oncustomized fractal zone plates", *Laser Physics Letters* **10**, 035003 (2013).

[Tebaldi09] M. Tebaldi, W. D. Furlan, R. Torroba, y N. Bolognini, “Optical-data storage-readout technique based onfractal encrypting masks", *Optical Letters* **34**, 316–318 (2009).

[Tonouchi07] M. Tonouchi, “Cutting-edge terahertz technology", *Nature Photonics* **1**, 97–105 (2007).

[Tsao14] C. W. Tsao, Y. H. Cheng y W. J. Hsueh, “Localized modes in one-dimensional symmetric Thue-Morse quasicrystals”, *Optics Express* **22**, 24378–24383 (2014).

[Turitsyn07] S. K. Turitsyn, V. K. Mezentsev, M. Dubov, A. M. Rubenchik y M. P. Fedoruk, “Sub-critical regime of femtosecond inscription”, *Optical Express* **15,** 14750 (2007).

[Verma14a] R. Verma, M. K. Sharma, P. Senthilkumaran, y V. Banerjee, “Analysis of Fibonacci gratings y theirdiffraction patterns", *Journal of the Optical Society of America A* **31**, 1473–1480 (2014)

[Verma14b] R. Verma, V. Banerjee, y P. Senthilkumaran, “Fractal signatures in the aperiodic Fibonacci grating", *Optical Letters* **39**, 2557–2560 (2014).

[Vyas07] S. Vyas y P. Senthikumaran, “Interferometric optical vortex array generator”, *Applied Optics* **46**, 2893–2898 (2007).

[Walsh23] J. L. Walsh, “A closed set of normal orthogonal functions", *American Journal of Mathematics* **45**, 5–24 (1923).

[Wan12] J. Wang, J. Y. Yang, I. M. Fazal, N. Ahmed, Y. Yan, H. Huang, Y. Ren, Y. Yue, S. Dolinar, M. Tur, y A. E. Willner, “Terabit freespace data transmission employing orbital angular momentum multiplexing", *Nature Photonics* **6**, 488–496 (2012).

[Wan16] J. Wang, "Advances in communications using optical vortices", *Photonics Research* **4**, B14-B28 (2016).

[Wang02] S. Wang et al., “Characterization of T-ray binary lenses", *Optical Letters* **27**, 1183–1185, (2002).

[Wang13] X. Wang, Z. Xie, W. Sun, S. Feng y . Cui, J. Ye y Y. Zhang, “Focusing y imaging of a virtual all-optical tunable terahertz Fresnel zone plate", *Optics Letters* **38**, 4731–4734 (2013).

[Watts14] C. M. Watts et al., “Terahertz compressive imaging with metamaterial spatial light modulators", *Nature Photonics* **8**, 605–609 (2014).

[Wei15] X. Wei, C. Liu, L. Niu, Z. Zhang, K. Wang, Z. Yang, y J. Liu, “Generation of arbitrary order Bessel beams via 3D printed axicons at the terahertz frequency range", *Applied Optics* **54**, 10641–10649 (2015).

[Wilk09] R. Wilk, N. Vieweg, O. Kopschinski y M. Koch, “Liquid crystal based electrically switchable Bragg structure for THz waves”, *Optics Express* **17**, 7377 (2009).

[Willner15] A. E. Willner, et al., “Optical communications using orbital angular momentum beams", *Advances in Optics y Photonics* **7**, 66–106 (2015).

[Withington04] S. Withington, “Terahertz astronomical telescopes y instrumentation", *Philosophical Transactions of the Royal Society A: Mathematical, Physical y Engineering Sciences* **362**, 395–402 (2004).

[Wu16] K. Wu y G. P. Wang, “Two-dimensional Fibonacci grating for far-field super-resolution imaging", *Scientific Reports* **6**, 38651 (2016).

[Xie13] Z. Xie, X. Wang, J. Ye, S. Feng, W. Sun, T. Akalin, y Y. Zhang, “Spatial terahertz modulator", *Scientific Reports* **3**, 3347 (2013).

[Yadav15] A. K. Yadav, S. Vashisth, H. Singh, y K. Singh, “A phase-image watermarking scheme in gyrator domainusing devil’s vortex Fresnel lens as a phase mask", *Optics Communications* **344**, 172–180 (2015).

[Yang14] Y. Yang, W. Wang, P. Moitra, I. Kravchenko, D. Briggs y J. Valentine, “Dielectric meta reflect array for broadby linear polarization conversion y optical vortex generation”, *Nano Letters* **14**, 1394–1399 (2014).

[Yu09] Y. Yu y W. Dou, “Generation of pseudo-Bessel beams at THz frequencies by use of binary axicons", *Optics Express* **17**, 888–893 (2009).

[Yu15] S. Yu, “Potentials y challenges of using orbital angular momentum communications in optical interconnects", *Optics Express* **23**, 3075–3087 (2015).

[Zhang10] B. Zhang, D. Zhao, “Square Fresnel zone plate with spiral phase for generating zero axial irradiance”, *Optics Letters* **35,** 1488-1490 (2010).

[Zhang12] Q. Zhang, J. Wang, M. Wang, J. Bu, S. Zhu, B. Z. Gao, y X. Yuan, “Depth of focus enhancement of amodified imaging quasi-fractal zone plate", *Optics & Laser Technology* **44**, 2140–2144 (2012)

[Zheng18] C. Zheng, H. Zang, Y. Du, Y. Tian, Z. Ji, J. Zhang, Q. Fan, C. Wang, L. Cao y E. Liang, “Realization of arbitrarily long focus-depth optical vortices with spiral area-varying zone plates”, *Optics Communications* **414**, 128-133 (2018).

[Zhou12] Y. Zhou, K. Panetta, S. Agaian y C. P. Chen, “Image encryption using P-Fibonacci transform y decomposition”, *Optics Communications* **285**, 594-608 (2012).